PREPARATION AND PROPERTIES OF PVDF BASED $BaTiO_3$ CONTAINING NANOCOMPOSITES

by

TLADI GIDEON MOFOKENG (B.Sc. Hons.)

Submitted in accordance with the requirements for the degree

MASTER OF SCIENCE (M.Sc.)

Department of Chemistry

Faculty of Natural and Agricultural Sciences

at the

UNIVERSITY OF THE FREE STATE (QWAQWA CAMPUS)

SUPERVISOR: PROF A.S. LUYT
CO-SUPERVISOR: DR V. DJOKOVIĆ

January 2014

DECLARATION

I hereby declare that the research in this thesis is my own independent work, and has not previously been submitted to any other University in order to obtain a degree. I further cede copyright of the dissertation in favour of the University of the Free State.

_____

T.G. Mofokeng

DEDICATION

This work is dedicated to my father (Mokudinyana Johannes Mofokeng), my mother (Mmatomatsi Emily Mofokeng), my grandmother (Mampaea Eva Khumalo), my son (Manti Lehakwe Mofokeng) and the entire Mofokeng family. Your love will always be engraved in my heart for as long as I live.

To my brothers, sister and fiancee, Ramotseng Mofokeng, Matjiki Mofokeng, Mokgafola Mofokeng and Konoswang Rabohlale. Thank you for all that you are to me. Words cannot express my love for you.

To my nephews and niece, Bohlokwa Mofokeng, Rorisang Mofokeng and Sebabatso Mofokeng. Always remember to respect the elders and your days shall be longer. Out of nowhere God will put you somewhere.

Ke thelleng, nna Mofokeng wa Makara, Manti wa Mmope. Motho wa maotwana finyela. Maoto a makalo ka dinaledi.

ABSTRACT

The β-crystallization of PVDF was investigated in this study. Nanocomposites were prepared by melt mixing PVDF, and 80/20 w/w PVDF/PMMA blends, with non-activated and (5 and 10 min) mechanically activated $BaTiO_3$ nanoparticles. The samples were then quenched in ice water followed by annealing at 80 °C for 24 hours. The sizes of the $BaTiO_3$ particles were reduced through mechanical activation prior to mixing, and the activated $BaTiO_3$ nanoparticles interacted better with the polymer matrix. The $BaTiO_3$ nanoparticles were well dispersed in the polymer matrix, but also formed agglomerates. The β-phase was only detected in the blend and the blend nanocomposites. The non-activated $BaTiO_3$ nanoparticles favoured the α-phase crystallization of PVDF/PMMA, while the mechanically activated nanoparticles induced the β-phase. The thermal stabilities of PVDF and the PVDF/PMMA blend decreased with the addition of $BaTiO_3$ nanoparticles. At a fixed filler content, the storage modulus and dielectric constant increased with an increase in activation time. The crystallization and melting temperatures of the matrix were slightly affected by the introduction of activated $BaTiO_3$ particles.

LIST OF ABBREVIATIONS AND SYMBOLS

α_a	relaxation associated with motion of amorphous regions
α_c	relaxation associated with motion of crystalline regions
DMA	dynamic mechanical analysis
DSC	differential scanning calorimetry
ΔH_c	crystallization enthalpy
ΔH^n_c	normalized crystallization enthalpy
ΔH_m	melting enthalpy
ΔH^n_m	normalized melting enthalpy
E’	storage modulus
E”	loss modulus
ε	dielectric constant
ε’	dielectric permittivity
ε”	dielectric loss
FTIR	Fourier-transform infrared
LO	longitudinal optical mode
M_w	molecular weight
MFI	melt flow index
MG	functionalized graphene
MWNT	multi-walled carbon nanotube
PMMA	poly(methyl methacrylate)
PVDF	poly(vinylidene fluoride)
SEM	scanning electron microscopy
$T_{10\%}$	decomposition temperature at 10% mass loss
$T_{50\%}$	decomposition temperature at 50% mass loss
T_{crit}	critical temperature
T_c	crystallization temperature
T_g	glass transition temperature
T_m	melting peak temperature
TGA	thermogravimetric analysis
TO	transverse optical mode
T_{on}	onset temperature of degradation
Tan δ	damping factor
XRD	x-ray diffractometry

TABLE OF CONTENTS

LIST OF TABLES

LIST OF FIGURES

Page

CHAPTER 1

GENERAL INTRODUCTION

1.1. Background

Piezoelectricity can be defined as the ability of certain materials to expand or contract under the influence of an applied electric field. Examples of piezoelectric materials include quartz, barium, strontium, and some polymers such as PVDF. The use of poly(vinylidene fluoride) (PVDF) in piezoelectric or dielectric applications has attracted much interest over the past decades. PVDF is a polymorphic, semi-crystalline polymer which crystallizes into at least four crystallographic phases, namely the α-, γ- and δ-phases, but most importantly the β-phase. Each phase of PVDF has a specific conformation, and it is possible to transform from one phase to the other [1-4]. The α-phase of PVDF has a monoclinic unit cell and is the most stable phase from a thermodynamic point of view. This polymorph is non-polar, piezoelectrically inactive, and has a TGTGT' conformation in which T and G are the trans and gauche chain conformations, respectively. In the α-polymorph, the chains are packed in the unit cell in such a way that the molecular dipoles are anti-parallel and there is no net (crystal) dipole [5]. The α-phase of PVDF is obtained by slow cooling from the melt or quenching at temperatures greater than 30 °C [6]. The γ-phase is polar and has an orthorhombic unit cell with a TTTGTTTG' conformation. This polymorph can be obtained by crystallization from some highly polar solvents, high temperature annealing, or high pressure crystallization. The γ-phase is an intermediate phase between the α and β-phases [7]. The δ-phase is a polar phase of the α-phase. This phase has been identified as one having the same chain conformation as the α-phase, but the carbon-fluorine bonds are aligned in one direction around the chain direction and every other chain is rotated, resulting in a net dipole [8].

Over the past years, the β-phase of PVDF has attracted much interest because it is the one giving PVDF the piezo, pyro and dielectric properties. In the β-phase, PVDF is used in applications such as capacitors, sensors, and actuators [9-13]. The β-phase is polar and has a TTTT' conformation in which all the fluorine atoms are located on the same side of the polymer chain [14,15]. However, the fluorine and hydrogen atoms in the β-phase are on the opposite sides of the polymer backbone, resulting in a non-zero dipole moment. It is very

challenging to induce the β-phase in PVDF, and this phase can be induced from other phases of PVDF under appropriate conditions and methods, or a combination of both. These include stretching/drawing, quenching, polymer blending and the incorporation of fillers. The oriented β-phase can be obtained from the α-phase by stretching/drawing the PVDF film. A maximum fraction of an oriented β-phase is achieved at a stretch ratio of five and a temperature of 80 °C, whereas the unoriented β-phase can be obtained by rapid quenching from the melt. The critical quenching temperature for β-phase formation was reported to be 30 °C. Quenching PVDF at temperatures below 30 °C results predominantly in the β-phase, while above this temperature (30 °C) the α-phase dominates [16-18]. A quenching temperature below 30 °C must be selected with caution, because quenching at temperatures lower than 0 °C, as in the case of liquid nitrogen, may result in a highly brittle β-phase PVDF film with cracks, thus limiting the applications of this material. Subsequent annealing of the quenched PVDF results in an improvement of the β-phase [19]. The β-phase PVDF cannot be used for applications requiring high temperatures, because high temperatures destroy the β- crystals thus giving rise to α-crystals during cooling to room temperature [6].

Polymer blending is an essential method for producing polymeric materials from existing polymers. A polymer blend is a mixture of at least two polymers or copolymers. The advantages of polymer blending include cost effectiveness and less time-consumption than the development of new monomers as the basis for new polymeric materials. Additionally, a wide range of material properties is within reach by merely changing the blend composition [20]. In addition to its polymorphic character, another interesting aspect of PVDF is its ability to form blends that are miscible or partially miscible with certain carbonyl group containing polymers, such as polyacrylates, polyketones and polyacetates [21]. The miscibility of PVDF with carbonyl containing polymers is thought to occur through the dipole/dipole interaction between the $>CF_2$ groups of PVDF and the >C=O groups of the above-mentioned polymers, and to the hydrogen bonding between the double bonded oxygen of the carbonyl group or the acidic hydrogen of the $-CH_2-CF_2-$ group [22-24]. PMMA was, however, blended with PVDF in this study because of its ability to force PVDF to crystallize in the β-phase when quenched from the melt at PMMA contents of less than 30 wt.% [25,26]. This is attributed to the reduction of the crystallization rate of the α-phase with the incorporation of PMMA, which in turn makes quenching more efficient thus increasing the crystallinity of the β-phase crystals [26].

Another way of obtaining the β-phase of PVDF is by the inclusion of small amounts of fillers such as clay, TiO_2, and carbon nanotubes [27-29]. In the presence of the filler, PVDF chains bind onto the surface of the filler particles which forces them to crystallize in the β-phase. As the sizes of the fillers become smaller, large specific surfaces and defects form which improves the process [5,28,30-32]. For these reasons mechanical activated $BaTiO_3$ is a good filler because it possesses a large surface area and many defects to improve β-phase formation. This $BaTiO_3$ still maintains the tetragonal structure it had before activation [33].

Piezoelectricity in potential piezoelectric materials can be optimized by a poling process [34,35], which is achieved by putting a material in a constant electric field to force the dipoles to align in the same direction.

1.2. Aims and objectives of the study

The main objective of this study was to prepare and characterize polymer nanocomposites with piezoelectric properties. This is mainly achieved by β-phase nucleation of PVDF after melt mixing it with 20 wt.% PMMA, quenching in ice water and subsequent annealing. PVDF and PMMA were selected because of their high compatibility. The efficiency of non-activated and mechanically activated $BaTiO_3$ to induce β-phase formation on PVDF and 80/20 w/w PVDF/PMMA was also investigated. The idea was to incorporate piezoelectric nanofillers in a polymer matrix to increase its dielectric constant. The morphologies of the samples and the development of a β-phase were investigated using Fourier-transform infrared spectroscopy (FTIR), Raman spectroscopy, X-ray diffractometry (XRD) and scanning electron microscopy (SEM). The thermomechanical and thermal properties of the nanocomposites were investigated by using dynamic mechanical analysis (DMA), thermogravimetric analysis (TGA), and differential scanning calorimetry (DSC). The dielectric properties were investigated by using a dielectric spectroscopy.

1.3. Outline of the thesis

The layout of the thesis is as follows:

- Chapter 1: General introduction
- Chapter 2: Literature review
- Chapter 3: Materials and methods
- Chapter 4: Results and discussion
- Chapter 5: Conclusions

1.4. References

[1] A. Salimi, A.A. Yousefi. Conformational changes and phase transformation mechanisms in PVDF solution-cast films. Journal of Polymer Science: Part B: Polymer Physics 2004; 42:3487-3495.
DOI: 10.1002/polb.20223

[2] Y. Zhang, S. Jiang, M. Fan, Y. Zeng, Y. Yu, J. He. Piezoelectric formation mechanisms and phase transformation of poly(vinylidene fluoride)/graphite nanosheets nanocomposites. Journal of Materials Science: Materials in Electronics 2013; 24:927-932.
DOI: 10.1007/s10854-012-0851-1

[3] V.F. Cardoso, C.M. Costa, G. Minas, S. Lanceros-Mendez. Improving the optical and electroactive response of poly(vinylidene fluoride-trifluoroethylene) spin-coated films for sensor and actuator applications. Smart Materials and Structures 2012; 21:1-9.
DOI: 10.1088/0964-1726/21/8/085020

[4] W. Li, L. Yu, Y. Zhu, D. Hua, J. Wang, L. Luo, J. Zhang. Annealing effect on poly(vinylidene fluoride/trifluoroethylene) (70/30) copolymer thin films above the melting point. Journal of Applied Polymer Science 2010; 116:663-667.
DOI: 10.1002/app.31631

[5] S. Manna, S.K. Batabyal. A.K. Nandi. Preparation and characterization of silver-poly(vinylidene fluoride) nanocomposites: Formation of piezoelectric polymorph of poly(vinylidene fluoride). Journal of Physical Chemistry B 2006; 110:12318-12326.
DOI: 10.1021/jp061445y

[6] C-H. Du, B-K. Zhu, Y-Y. Xu. The effects of quenching on the phase structure of vinylidene fluoride segments in PVDF-HFP copolymer and PVDF-HFP/PMMA blends. Journal of Materials Science 2006; 41:417-421.
DOI: 10.1007/s10853-005-2182-6

[7] L. Priya, J.P. Jog. Polymorphism in intercalated poly(vinylidene fluoride)/clay nanocomposites. Journal of Applied Polymer Science 2003; 89:2036-2040.
DOI: 10.1002/app.12346

[8] B. Mohammadi, A.A. Yousefi, S.M. Bellah. Effect of tensile strain rate and elongation on crystalline structure and piezoelectric properties of PVDF thin films. Polymer Testing 2007; 26:42-50.
DOI: 10.1016/j.polymertesting.2006.08.003.

[9] X. Qiu. Patterned piezo-, pyro-, and ferroelectricity of poled polymer electrets. Journal of Applied Physics 2010; 108:1-20.
DOI: 10.1063/1.3457141

[10] S. Sokhanvar, M. Packirisamy, J. Dargahi. A multifunctional PVDF-based tactile sensor for minimally invasive surgery. Smart Materials and Structures 2007; 16:989-998.
DOI: 10.1088/0964-1726/16/4/006

[11] Z. Chen, Y. Shen, N. Xi, X. Tan. Integrated sensing for ionic polymer-metal composite actuators using PVDF thin films. Smart Materials and Structures 2007; 16:262-271.
DOI: 10.1088/0964-1726/16/2/S10

[12] T. Hanemann, B. Schumacher. Realization of embedded capacitors using polymer matrix composites with barium titanate as high-k-active filler. Microsystem Technologies 2012; 18:745-751.
DOI: 10.1007/s00542-012-1458-4

[13] A.M. Othman, M.S. El-Shahawi, M. Abdel-Azeem. A novel barium polymeric membrane sensor for selective determination of barium and sulphate ions based on the complex ion associate barium(II)-Rose Bengal as neutral ionophore. Analytica Chimica Acta 2006; 555:322-328.
DOI: 10.1016/j.aca.2005.09.016

[14] Y.Y. Zhang, S.L. Jiang, Y. Yu, G. Xiong, Q.F. Zhang, G.Z. Guang. Phase transformation mechanisms and piezoelectric properties of poly(vinylidene fluoride)/montmorillonite composite. Journal of Applied Polymer Science 2012; 123:2595-2600.

DOI: 10.1002/app.34431

[15] L.L. Sun, B. Li, Z.G. Zhang, W.H. Zhong. Achieving very high fraction of β-crystal PVDF and PVDF/CNF composites and their effect on AC conductivity and microstructure through a stretching process. European Polymer Journal 2010; 46:2112-2119.
DOI: 10.1016/j.eurpolymj.2010.09.003

[16] V. Sencadas, R. Gregorio Jr, S. Lanceros-Méndez. α to β phase transformation and microestructural changes of PVDF films induced by uniaxial stretch. Journal of Macromolecular Science Part B. Physics 2009; 48:514-525.
DOI: 10.1080/00222340902837527

[17] D. Yang, Y. Chen. β-phase formation of poly(vinylidene fluoride) from the melt induced by quenching. Journal of Materials Science Letters 1987; 6:599-603.
DOI: 10.1007/BF01739296

[18] K.J. Kim, Y.J. Cho, Y.H. Kim. Factors determining the formation of β crystalline phase of poly(vinylidene fluoride) in poly(vinylidene fluoride)-poly(methyl methacrylate) blends. Vibrational Spectroscopy 1995; 9:147-159.
DOI: 10.1016/0924-2031(94)00092-U

[19] S. Satapathy, S. Pawar, P.K. Gupta, K.B.R. Varma. Effect of annealing on phase transition in poly(vinylidene fluoride) films prepared using polar solvent. Bulletin of Materials Science 2011; 34:727-733.
DOI: 10.1007/s12034-011-0187-0

[20] C. Koning, M. van Duin, C. Pagnoulle, R. Jerome. Strategies for compatibilization of polymer blends. Progress in Polymer Science 1998; 23:707-757.
DOI: 10.1016/S0079-6700(97)00054-3.

[21] M.M. Abolhasani, Q. Guo, A. Jalali-Arani, H. Nazockdast. Poly(vinylidene fluoride)-acrylic rubber partially miscible blends: Phase behavior and its effects on the mechanical properties. Journal of Applied Polymer Science 2013; 129:1-12.
DOI: 10.1002/app.39213

[22] M. Li, N. Stingelin, J.J. Michels, M-J. Spijkman, K. Asadi, K. Feldman, P.W.M. Blom, D.M. de Leeuw. Ferroelectric phase diagram of PVDF: PMMA. Macromolecules 2012; 45:7477-7485.
DOI: 10.1021/ma301460h

[23] I.S. Elashmawi, N.A. Hakeem. Effect of PMMA addition on characterization and morphology of PVDF. Polymer Engineering and Science 2008; 48:895-901.
DOI: 10.1002/pen.21032

[24] W. Ma, S. Chen, J. Zhang, X. Wang. Crystallization behavior and hydrophilicity of poly(vinylidene fluoride) (PVDF)/poly(methylmethacrylate) (PMMA)/poly(styrene-co-acrylonitrile) (SAN) ternary blends. Colloid and Polymer Science 2009; 287:147-155.
DOI: 10.1007/s00396-008-1958-z

[25] H. Song, S. Yang, S. Sun, H. Zhang. Effect of miscibility and crystallization on the mechanical properties and transparency of PVDF/PMMA blends. Polymer-Plastics Technology and Engineering 2013; 52:221-227.
DOI: 10.1080/03602559.2012.735314

[26] R. Gregorio Jr, N.C. Pereira de Souza Nociti. Effect of PMMA addition on the solution crystallization of the alpha and beta phases of poly(viny1idene fluoride) (PVDF). Journal of Physics D: Applied Physics 1995; 28:432-436.
DOI: 10.1088/0022-3727/28/2/028

[27] G. Murasawa, A. Nishioka, K. Miyata, T. Koda, H. Cho. Electrically excited oscillation and crystalline structure of a nanoclay/poly(vinylidene fluoride) composite film. Journal of Intelligent Material Systems and Structures 2011; 22:2103-2112.
DOI: 10.1177/1045389X11425283

[28] S. Yu, W. Zheng, W. Yu, Y. Zhang, Q. Jiang, Z. Zhao. Formation mechanism of β-phase in PVDF/CNT composite prepared by the sonication method. Macromolecules 2009; 42:8870-8874.
DOI: 10.1021/ma901765j

[29] J.G. Lee, S.H. Kim. Structure development of PVDF/PMMA/TiO_2 composite film with casting conditions. Macromolecular Research 2011; 19:72-78.
DOI: 10.1007/s13233-011-0109-4

[30] S. Manna, A.K. Nandi. Piezoelectric β polymorph in poly(vinylidene fluoride)-functionalized multiwalled carbon nanotube nanocomposite films. The Journal of Physical Chemistry C 2007; 111:14670-14680.
DOI: 10.1021/jp073102l

[31] M. El Achaby, F-E. Arrakhiz, S. Vaudreuil, E.M. Essassi, A. Qaiss, M. Bousmina. Nanocomposite films of poly(vinylidene fluoride) filled with polyvinylpyrrolidone-

coated multiwalled carbon nanotubes: Enhancement of β-polymorph formation and tensile properties. Polymer Engineering and Science 2013; 53:34-43.
DOI: 10.1002/pen.23236

[32] J. Sheth, D. Kumar. Silicon carbide-induced piezoelectric β-phase in poly(vinylidene fluoride) and its properties. Journal of Materials Research 2012; 27:1838-1845.
DOI: 10.1557/jmr.2012.117

[33] V.P. Pavlović, D. Popović, J. Krstić, J. Dojčilović, B. Babić, V.B. Pavlović. Influence of mechanical activation on the structure of ultrafine $BaTiO_3$ powders. Journal of Alloys and Compounds 2009; 486:633-639.
DOI: 10.1016/j.jallcom.2009.07.008

[34] V. Sencadas, S. Lanceros-Méndez, J.F. Mano. Characterization of poled and non-poled β PVDF films using thermal analysis techniques. Thermochimica Acta 2004; 424:201-207.
DOI: 10.1016/j.tca.2004.06.006

[35] M. Marsilius, T. Granzow, J.L. Jones. Effect of electrical and mechanical poling history on domain orientation and piezoelectric properties of soft and hard PZT ceramics. Science and Technology of Advanced Materials 2011; 12:1-8.
DOI: 10.1088/1468-6996/12/1/015002

CHAPTER 2

LITERATURE REVIEW

2.1 Barium titanate ($BaTiO_3$) nanoparticles

A number of studies have been done on ceramics, especially their use as fillers for polymeric materials [1-3]. The purposes of incorporating fillers were to either reinforce or improve the dielectric properties of polymer matrices. With this in mind, the ceramic filler of particular interest is barium titanate due to its remarkable ferroelectric properties, which are essential in the electronic industries, and its environmental friendliness when compared to lead containing ceramics such as lead titanium zirconate. $BaTiO_3$ has a critical temperature (T_{crit}) of 120-130 °C and a perovskite structure, which is an ideal cube. The perovskite cubic structure is stable above T_{crit}, but transforms to a hexagonal structure around 1460 °C. The cubic structure also transforms to a tetragonal structure on cooling to temperatures between T_{crit} and 0 °C [4,5]. The tetragonal phase of $BaTiO_3$ is very important because of its large dielectric constants, which are required in the electronics industry.

Over the past decades, a number of methods have been proposed for synthesizing $BaTiO_3$, namely sol-gel, solid state reaction, hydrothermal, co-precipitation and the polymeric precursor method [4]. The most commonly used methods for $BaTiO_3$ synthesis are the solid state reaction and hydrothermal methods [4,6-9]. During a solid state reaction $BaTiO_3$ is produced by reacting solid barium carbonate with titania, and calcinating the mixture at 700-1200 °C [4,6]. This method results in large $BaTiO_3$ nanoparticles that are highly agglomerated and have poor electrical properties [6]. Due to the miniaturization of electronic devices there is a large demand for nanosized $BaTiO_3$. To achieve this, intensive ball milling over long periods of time during the reaction is employed [10-12]. Even though this method seems to serve the purpose of obtaining fine $BaTiO_3$ nanoparticles, it cannot be easily implemented on a laboratory scale because it requires sophisticated equipment.

The hydrothermal method involves heating an aqueous suspension of insoluble salts in a closed system, i.e an autoclave, at a moderate temperature and pressure so that the formation of the desired phase occurs. Unlike the solid state reaction method, the hydrothermal method

ensures the production of $BaTiO_3$ in a single processing step and does not require sophisticated equipment. In the synthesis of $BaTiO_3$ by the hydrothermal method, fine $BaTiO_3$ nanoparticles with an average size of less than 200 nm were obtained [7-9].

2.2 Poly(vinylidene fluoride) (PVDF)

PVDF is a fascinating fluoropolymer which is used in many applications because of its good thermal stability, and excellent mechanical, weathering, chemical and processing properties. Its outstanding mechanical strength and excellent chemical resistance make it suitable for wastewater treatment where it is used as a membrane for filtering water. Its weathering resistance ensures it is a material of choice for use in coatings. The good thermal stability of PVDF is attributed to the high electronegativity of the fluorine atoms situated on the chain and the high bond dissociation energy of the C−F bonds. PVDF undergoes thermal degradation to primarily yield hydrogen fluoride. Other chemical reactions such as crosslinking of the polymer and the formation of carbon-carbon double bonds may occur during the thermal degradation [13]. Several studies [14-17] investigated the thermal degradation of PVDF by using thermogravimetric analysis and pyrolysis. In these studies, the TGA curves showed a single degradation step and a char residue beyond the degradation temperature. The single degradation step is caused by the dehydrofluorination of hydrogen fluoride in PVDF. However, there is a study where the TGA curves of PVDF showed double degradation steps, which were attributed to dehydrofluorination, and the formation of a double bonded $C_4H_3F_3$ [18].

PVDF is a polymorphic, semi crystalline polymer that crystallizes in at least four crystallographic phases, namely alpha (α), gamma (γ), delta (δ), and most importantly the beta (β) phase. The β-phase is of prime importance because of its high dielectric constant, as well as piezoelectric and pyroelectric properties, which are essential in the electronics industry. Many studies have been devoted to transforming PVDF from its stable α-phase to the unstable β-phase [19-21]. It has been shown that mechanical drawing of the α-phase PVDF at stretch ratios of 4 and 5 at 80 °C results in the maximum amount of β-phase as detected by FTIR [19,20]. The authors attributed this transformation to a change from a spherulitic to a micro fibrillar structure, which induced an all-trans planar zigzag conformation into the crystals. However, the β-phase has also been obtained by annealing the γ-phase PVDF attained by

casting in dimethyl sulfoxide [21]. The maximum β-phase was attained when annealing was performed at 90 °C for 5 hours as seen on Raman spectroscopy and FTIR. The authors attributed the observed results to a decrease in viscosity of the PVDF, which in turn increased the chain mobility. Consequently, the thermal energy was sufficient to reorganize the structure of conformers from the TTTGTTTG' sequence of the γ-phase to the TTTTTTTT' sequence of the β-phase.

2.3 PVDF nanocomposites

2.3.1 Morphology and polymorphic phases

The most commonly used methods for preparing PVDF nanocomposites are solution mixing and melt mixing. Unlike melt mixing, solution mixing promotes improved dispersion of the filler in the PVDF matrix. The dispersion of the filler in the polymer matrix and the morphology of the resulting polymer nanocomposites are highly significant because they serve as a basis for predicting how the material will perform. The morphology and crystalline phases of PVDF nanocomposites are normally investigated using scanning electron microscopy (SEM), transmission electron microscopy (TEM), optical microscopy, Fourier-transform infrared (FTIR) spectroscopy, Raman spectroscopy and X-ray powder diffractometry (XRD). Studies on the dispersion of $BaTiO_3$ in PVDF/$BaTiO_3$ nanocomposites prepared by solution mixing and long sonication times revealed non-agglomerated and well dispersed nanoparticles in the polymer matrix [22-24]. However, the dispersion in a composite with 20 vol.% investigated in [25] was not homogenous. The authors reported that the volume fraction of PVDF in the composite was high and that the PVDF had not been absorbed, resulting in an inhomogeneous dispersion of $BaTiO_3$ nanoparticles in the composite. Their reason seems to be inadequate, since a total sonication time of 30 minutes was used, while other authors used sonication times far greater than 30 minutes and obtained homogenously dispersed nanocomposites at that content [22,23].

Several researchers [26-29] investigated the morphologies of a number of PVDF nanocomposites. Generally, PVDF crystallized exclusively in the α-phase. However, the size of the α-phase spherulites decreased with the addition of nanofillers. It is generally expected that the addition of nanofillers in PVDF induces the β-phase at the expense of the α-phase.

This is attributed to the nanofillers disrupting the α-phase crystallization process. These studies confirm what is already known that the β-phase in PVDF is induced by the incorporation of nanofillers. Similar behaviour was observed on addition of silica microparticles [30]. The sizes of the spherulites decreased with an increase in silica content. However, in this case the microparticles did not induce the β-phase. This may be due to the size of the filler and the lack of defects. These properties play a major role in binding PVDF chains tightly to the particles in order to induce the β-phase.

2.3.2 Thermal properties

The thermal properties of a polymeric material are important because they give information about conditions that a material has to bear before failure. Unlike metallic materials, polymeric materials have a low use temperature, which reduces their use in making certain products. A good solution is to incorporate nanofillers to improving their thermal properties. In the automotive industry, most car manufacturers are now using nanocomposite materials instead of metallic materials for making body panels. This results in a car with light body panels and thus less fuel consumption. DSC and TGA are the most used techniques for investigating the thermal properties of nanocomposites [18,30-33]. Studies on the thermal stabilities of PVDF nanocomposites reveal that the thermal stability and char content of PVDF increased with an increase in nanosilica content [30-32]. The increase in the thermal stability was attributed to the good dispersion and thermal transmission properties that enable the silica nanoparticles to strongly hinder the volatility of the decomposed products and thus limit the continuous decomposition. There is a study in which the thermal stability of PVDF decreased with increases in the filler content [18]. The decrease in the thermal stability was attributed to a decrease in the surface area caused by an increase in the size of the filler as its content increased. In another study the decrease in the thermal stability with an increase in nanofiller content was ascribed to the catalytic effect of the nanofillers [33].

Various studies on PVDF nanocomposites have been conducted for analyzing the effect of the addition of different fillers on the melting characteristics [14,18,29,34,35]. In these studies, the nanocomposites displayed either a single or a double melting peak. The double melting peaks were related to either the melting of crystals with different sizes or to polymorphism. Generally, the authors stated that this phenomenon was due to polymorphism, which was attested by their XRD and FTIR results confirming the presence of both α- and β-phases.

They also stated that the α-phase crystals melt at temperatures lower than the β-phase crystals. A single melting peak, which shifted to higher temperatures as the nanoparticle content increased, was attributed to the development of β-phase crystals [18,29,34,35]. Other studies on PVDF nanocomposites, however, revealed that the melting point of PVDF decreased with an increase in the filler content [36,37]. Since PVDF displayed only the α-phase, the authors assumed that the decrease in melting temperature was due to the presence of or increase in the β-phase, which was detected by FTIR and XRD. They also mentioned that the β-phase crystals melt at lower temperatures than the α-phase crystals, which is contrary to what the previously mentioned authors stated.

2.3.3 Mechanical properties and thermomechanical behaviour

The mechanical and thermomechanical behaviour of PVDF nanocomposites are generally investigated by tensile testing and dynamic mechanical analysis (DMA), respectively. Tensile testing is normally performed at room temperature, whereas DMA is performed by heating polymers from very low temperatures to high temperatures. DMA studies on PVDF nanocomposites have been reported in a number of studies [18,33,38,39] in which various nanofillers were used. An overall increase in the storage modulus with an increase in the concentration of the nanofillers over the whole temperature range was observed. The increase in storage modulus was attributed to the reinforcing effect of the nanofillers due to their high aspect ratios. However, in some studies the nanocomposites with low filler content had higher storage modulus values than ones with high filler content, due to the better lattice packing at low content. An increase in the crystallinity of PVDF was also one of the reasons for the increase in storage modulus at low loadings.

The tensile properties of PVDF in various PVDF nanocomposites generally showed higher tensile modulus values compared to the pristine polymer due to the reinforcing effect and good dispersion of the nanofillers in PVDF [40,41]. However, in one study the modulus was lower at high filler loadings [40]. The authors did not mention the reason for these lower values. It is, however, known in the nanocomposites world that poor dispersion and agglomeration at higher filler loadings might have a detrimental effect on the tensile properties of the nanocomposites.

2.3.4 Dielectric properties of PVDF composites

Because of its high dielectric constant, barium titanate ($BaTiO_3$) is one material used for making ceramic capacitors. However, ceramic materials are brittle, suffer from low mechanical strength, and thus cannot be exposed to large electric fields [42]. To overcome this, polymers are often mixed with ceramics. The frequency dependences on the dielectric constants (ε) of PVDF/$BaTiO_3$ composites were investigated [22,23]. In both cases ε of the composites decreased with increases in frequencies, but a significant decrease was observed around a frequency of 3 x 10^5 Hz in study [22]. The authors attributed the large decrease to a dipole relaxation of the nanocomposites lagging behind the fast change of the applied field. Moreover, with reference to PVDF, the dielectric constant increased on addition of $BaTiO_3$. The high ε in the composites was attributed to the high ε of $BaTiO_3$. Studies on the dielectric properties of PVDF/carbon nanotubes showed increases in the dielectric constants as carbon nanotubes were incorporated, and the authors related it to the formation of capacitor networks [40,43]. The dielectric constants of PVDF/$BiCl_3$ and PVDF/graphite composites were also investigated [27,44]. An increase in ε was observed as graphite and $BiCl_3$ nanofillers were added. These results were attributed to the high dielectric constants and conductivities of the nanofillers, as well as the increase in the number of charge carriers.

2.4 Poly(methyl methacrylate) (PMMA)

Poly(methyl methacrylate) (PMMA) is an important member in the family of polyacrylic and methacrylic esters. It has several properties allowing it to be used in many applications. For example, its outstanding optical clarity allows it to be used as a replacement for glass. Because of its low toxicity and compatibility with human tissue, it is used for bone cements, contact and intraocular lenses, screw fixation in bone, filler for bone cavities and skull defects, and vertebrae stabilization in osteoporotic patients. On the other hand, PMMA shows poor abrasion resistance and thermal stability, which limits its use in certain applications [45]. Due to its low thermal stability, PMMA is used at temperatures less than 80 °C.

Over the past decades, a number of thermal degradation mechanisms of PMMA have been proposed [46-48]. However, PMMA is widely believed to undergo degradation by main chain random scission and homolytic scission [49]. During the degradation by main chain random

scission, PMMA primarily degradates to yield an isobutyryl macroradical and a primary macroradical. The isobutyryl macroradical further undergoes β-scission with the generation of methyl methacrylate monomers, while the primary macroradical is believed to undergo β-elimination with the formation of methallyl-terminated PMMA, CO, CO_2, methoxy and methyl radicals. In the homolytic scission of the methoxycarbonyl group, the remaining polymer radical can undergo β-scission to form an isobutyryl macroradical and a methallyl-terminated PMMA chain. The newly formed radical can then cleave to give another isobutyryl macroradical, which will depolymerize, and a series of small molecules, which depend upon the small radicals formed in the previous step [49]. However, the main product formed during the degradation of PMMA is methyl methacrylate irrespective of the degradation path followed [50].

2.5 PMMA nanocomposites

2.5.1 Morphology

A few studies have reported on PMMA/$BaTiO_3$ nanocompositers. In these studies, core-shell structures of PMMA/$BaTiO_3$ nanocomposites have been prepared via *in situ* atom transfer radical polymerization and free radical emulsion polymerization [51,52]. Generally, SEM results showed well embedded and homogenous dispersion of $BaTiO_3$ in the PMMA matrix. Additionally, no debonding was observed between the PMMA and $BaTiO_3$ nanoparticles. The effect of titania on the morphology of PMMA have been investigated in a number of studies [53-55]. In these studies, the nanocomposites were prepared by melt mixing, *in situ*, and graft polymerization. Generally, there was a uniform dispersion of titania nanoparticles in the PMMA. Unfortunately, the nanoparticles agglomerated in the matrix forming aggregates with diameters of several micrometers. The main challenge in the field of polymer nanocomposites is the prevention of aggregates because they transform nanofillers to behave like microfillers which might serve as weak reinforcing particles in certain instances. However, it was shown that bead milling modified titania (anatase) where a silane coupling agent was used as a modifier resulted in non-agglomerated titania in PMMA [56]. Recently, a study on rutile and anatase titania showed that in melt mixed PMMA/TiO_2 nanocomposites, the rutile titania system had smaller agglomerates than the anatase titania system [57]. Based on these studies

[56,57], it can be assumed that bead milling modified rutile titania might have offered a simple solution for preparing non-agglomerated PMMA/TiO_2 nanocomposites.

2.5.2 Thermal properties

A number of studies have reported the glass transition temperature (T_g) of PMMA composites using DSC [58-61]. In these studies, different types of clays and preparation methods were used. Generally, T_g increased with the incorporation of clay, irrespective of the preparation method. The authors attributed the behavior to the strong interaction between PMMA and clay, as well as the confinement of PMMA chains within the clay layers consequently restricting chain mobility. However, a sudden decrease in T_g at high clay loading was also observed, but a clear explanation for this behaviour was not given. The investigation of T_g using DSC in PMMA/TiO_2 nanocomposites has been the subject of many studies [53,55,62]. Generally, an increase in T_g with the incorporation of titania nanoparticles was observed and it was attributed to the strong interaction between PMMA and titania which decreased chain flexibility. However, increases in T_g were significant where methacrylic acid and 2-hydroxyethyl methacrylate were used as coupling agents for PMMA/TiO_2 systems [63,64]. The authors attributed the increases in T_g to the strong interfacial bonding between these coupling agents and PMMA. Interestingly, in the studies where 6-palmitate ascorbic acid (6-PAA) was used as a coupling agent, T_g decreased with increases in titania loading [65,66]. This was attributed to the plasticizing effect of TiO_2/6-PAA on PMMA.

The influence of zirconia on the thermal stability of PMMA has also been investigated [67,68]. Generally, the thermal stabilities improved with the incorporation of zirconia nanoparticles. The improvements in the thermal stabilities were attributed to the fact that zirconia nanoparticles trapped the generated free radicals during degradation, while resisting the out-diffusion of decomposition products in the process. The degradation of PMMA/ZrO_2 in nitrogen and air showed different degradation temperatures proving that degradation mechanisms are different in nitrogen and in air [69,70]. The incorporation of inorganic nanoparticles in polymer matrices is known as a simple way of improving the thermal stability of pure polymers. Nevertheless, it was found that the incorporation of rutile titania in PMMA had no significant effect on the thermal stability. The authors stated that the lower activation

energy in PMMA/TiO_2 (rutile) implied that rutile titania acted as a catalyst for thermal decomposition [57].

2.5.3 Mechanical properties and thermomechanical behaviour

Mechanical and thermomechanical investigation of PMMA/TiO_2 nanocomposites [62,71] showed a decrease in the tensile and dynamic modulus increased on filler loading. These observations were attributed to the stronger interfacial adhesion between PMMA and the titania nanoparticles through physiochemical interactions. Recently a study of melt mixed PMMA/TiO_2 showed that anatase titania immobilized the PMMA chains above T_g which shifted the storage modulus to higher values, whereas below T_g anatase titania had no influence on the storage modulus [57]. Interestingly, low contents of rutile titania (1 and 2 w.t%) plasticized the PMMA below T_g thus shifting the storage modulus to lower values, while effective immobilization of PMMA occurred above T_g at high rutile titania content (5 wt.%). Even though increases in storage modulus and T_g values were observed in [57], they were small compared to values reported in another study for a similar system [71]. Clearly, a detailed analysis of both studies is needed. Even though a good dispersion of titania in PMMA was observed in both studies, it is possible that the dispersion was much better in [71]. This can be attributed to a number of factors, i.e. the use of much smaller titania nanoparticles and more effective mixing methodology.

2.6 PVDF/PMMA blend and composites

2.6.1 Polymorphic phases and morphology

Blending PVDF with acrylic polymers such as PMMA is known to be another way of obtaining the desired polymorph of PVDF. Over the past decades, a number of studies have been done on PVDF/PMMA blends [72-76]. In these studies, PVDF/PMMA samples were either prepared by melt or solution mixing and more importantly quenched followed by annealing. The presence of the β-phase in the samples was detected using FTIR and XRD. Interestingly, in the studies where solution mixing was used for preparation [72,74], PVDF exhibited the β-phase which decreased in intensity on incorporation of PMMA. It seems like the presence of PMMA reduced the crystallization rate of the β-phase while promoting the α-

phase. However, a study on extruded and quenched PVDF/PMMA blends displayed PVDF exclusively in the α-phase [75]. An increase in PMMA content resulted in an α-phase reduction, which completely disappeared beyond 40 wt.% PMMA. The crystallization rate of the α-phase was reduced while β-phase formation was induced in the process. It is clear that PMMA can either reduce or improve the β-phase depending on the processing technique employed.

The effect of rutile titania on the polymorphic phases of PVDF in PVDF/PMMA extruded samples have been investigated [77,78]. In both studies, FTIR revealed that the addition of TiO_2 at low contents reduced the intensities of certain α-phase peaks (744 and 765 cm^{-1}) implying interaction between TiO_2 and PVDF in the blend composite system. The authors stated that the stable α-phase was changed to the unstable β-phase on addition of low contents of TiO_2 (< 30 wt.%). However, XRD showed that both the α- and β-phase were present at low contents, but one of the studies [78] revealed that incorporation of TiO_2 beyond 30 wt.% resulted in the disappearance of both phases.

Studies on the morphologies of PVDF/PMMA blends using optical microscopy and SEM also showed the presence of spherulites [72,74,75]. On addition of PMMA to PVDF, the sizes of the spherulites decreased and the number of spherulites increased due to reduced crystallization regions in PVDF. PMMA segregated into the interlamellar or intercrystalline regions of PVDF. At 80 wt.% PMMA and above, the spherulites disappeared but longitudinal shapes similar to PMMA were observed [74]. PVDF and PMMA are known to be miscible over a wide composition range. SEM micrographs of melt and solution mixed PVDF/PMMA blends over a wide composition range showed the absence of phase separation indicating miscibility [75,79]. The miscibility between PVDF and PMMA is due to the dipole/dipole interaction between the $>CF_2$ groups of PVDF and the >C=O groups of the above-mentioned polymers, and to the hydrogen bonding between the double bonded oxygen of the carbonyl group or the acidic hydrogen of the $-CH_2-CF_2-$ group.

SEM results of melt mixed PVDF/PMMA/TiO_2 composites showed that the incorporation of rutile TiO_2 at 2-5 wt.% contents results in homogenous dispersion and non-agglomeration of TiO_2 in the matrix, but aggregates of particles were observed at 10 wt.% TiO_2 [77]. Another study on extruded PVDF/PMMA/TiO_2 composites showed homogenous dispersion and non-

agglomeration of rutile TiO_2 at 5-15 wt.% contents, but aggregation of particles occurred at 30 wt.% [78]. The reason why aggregates are observed at higher contents may be related to the preparation method and the nanoparticle size. In study [78], an extrusion speed of 50 rpm and rutile TiO_2 of 210 nm diameter were used, whereas an extrusion speed of 30 rpm and rutile TiO_2 of 260-300 nm were used in study [77]. Clearly, higher extrusion speeds have a tendency of breaking aggregates into smaller aggregates and single particles.

2.6.2 Thermal properties

The effect of TiO_2 on the thermal degradation of PVDF/PMMA has also been investigated [77,78]. In these studies, the degradation of the blend composites displayed a single mass loss step compared to the pure blend, which displayed two mass loss steps. In the absence of TiO_2, PVDF/PMMA had an onset temperature of degradation (T_{on}) of 359 °C, while the incorporation of TiO_2 in the blend lowered T_{on} to 327 °C [77]. The decrease of T_{on} in the presence of TiO_2 was attributed to the metal oxide-catalyzed oxidative decomposition pathways in the composites and not to the degradation of TiO_2 since it is stable to temperatures above 600 °C. The blend had a residual char between 500-800 °C, and it was attributed to the formation of hydrogen fluoride, which led to unsaturation in the polymer backbone. This resulted in products that did not decompose easily. The residual char increased with the incorporation of TiO_2, which was attributed to a reaction between the chelating ligands of the titanium ion and hydrogen fluoride resulting in new products that were hard to decompose. However, study [78] revealed that the presence of TiO_2 in the blend increased the onset temperature of degradation (T_{on}), whereas a decrease in T_{on} with TiO_2 loading was observed in study [77]. It is not clear why the systems investigated in the two studies showed different behaviour, but maybe the particle size of TiO_2 played a role.

The α- and β-phases of PVDF have been reported to have different melting temperatures [14]. Even though α- and β-phases have been detected in melt mixed PVDF/PMMA/TiO_2, the melting curves displayed only single melting peaks in study [77], but double melting peaks in study [78]. The melting temperatures of the composites are the same as those of the blends in each study, but the crystallinity decreased with the addition of TiO_2. Another study on reduced graphene oxide-PMMA/PVDF composites showed that with the incorporation of poly(methyl methacrylate) functionalized graphene (MG), the melting peak of PVDF is split

into two peaks [17]. The authors attributed the low and high melting peaks to the melting of α- and β-crystals respectively. As the content of MG increased to 5 wt.%, only the high temperature melting peak was observed in the DSC curve implying that the β-phase was fully formed.

2.6.3 Mechanical properties and thermomechanical behaviour

The mechanical properties of PVDF/PMMA/TiO_2 nanocomposites have also been reported in studies [77] and [78]. Generally, increases in tensile strength and elongation at break were observed when TiO_2 was incorporated in the blend, but a maximum increase was reached at 2 and 10 wt.% TiO_2 in studies [77] and [78], respectively. The maximum improvement at these contents was attributed to the optimum dispersion of TiO_2 in the blend. Further addition of TiO_2 decreased the tensile strength and elongation at break. The authors attributed the decrease in mechanical properties to the defects caused by agglomeration of TiO_2, which in turn made stress concentrations to occur in PVDF/PMMA.

DMA was used to study the thermomechanical properties of PVDF/PMMA/carbon black composites [80]. In this study, the tan δ curves of PVDF/PMMA and PVDF/PMMA/carbon black showed a glass transition at similar temperatures. The authors found that carbon black had no influence on the glass transition temperature of the blend. A study on multi-walled carbon nanotube/poly(methyl methacrylate) (MWNT/PMMA) composites showed that the addition of 0.5 wt.% PVDF increased the storage modulus of MWNT/PMMA [81]. This was attributed to improved interfacial adhesion between MWNT and PMMA due to the presence of PVDF.

2.3. References

[1] E.-H. Kim, Y.-G. Jung, C.-Y. Jo. Microstructure and mechanical properties of heterogeneous ceramic-polymer composite using interpenetrating network. Journal of Nanomaterials 2012; 2012:1-6.
DOI: 10.1155/2012/932059

[2] K. Brandt, V. Salikov, H. Özcoban, P. Staron, A. Schreyer, L.A.S.A. Prado, K. Schulte, S. Heinrich, G.A. Schneider. Novel ceramic-polymer composites synthesized by

compaction of polymer-encapsulated TiO_2-nanoparticles. Composites Science and Technology 2011; 72:65-71.
DOI: 10.1016/j.compscitech.2011.10.001

[3] K. Osińska, D. Czekaj. Thermal behavior of BST/PVDF ceramic-polymer composites. Journal of Thermal Analysis and Calorimetry 2013; 113:69-76.
DOI: 10.1007/s10973-013-3026-2

[4] M.M. Vijatović, J.D. Bobić, B.D. Stojanović. History and challenges of barium titanate: Part 1. Science of Sintering 2008; 40:155-165.
DOI: 10.2298/SOS0802155V

[5] Y. Iqbal, A. Jamal, R. Ullah, M.N. Khan, R. Ubic. Effect of fluxing additive on sintering temperature, microstructure and properties of $BaTiO_3$. Bulletin of Materials Science 2012; 35:387-394.
DOI: 10.1007/s12034-012-0306-6

[6] S. Ohara, A. Kondo, H. Shimoda, K. Sato, H. Abe, M. Naito. Rapid mechanochemical synthesis of fine barium titanate nanoparticles. Materials Letters 2008; 62:2957-2959.
DOI: 10.1016/j.matlet.2008.01.083

[7] S.W. Lu, B.I. Lee, Z.L. Wang, W.D. Samuels. Hydrothermal synthesis and structural characterization of $BaTiO_3$ nanocrystals. Journal of Crystal Growth 2000; 219:269-276.
DOI: 10.1016/S0022-0248(00)00619-9

[8] X.H. Zhu, J.M. Zhu, S.H. Zhou, Z.G. Liu, N.B. Ming, D. Hesse. Microstructural characterization of $BaTiO_3$ ceramic nanoparticles synthesized by the hydrothermal technique. Solid State Phenomena 2005; 106:41-46.
DOI: 10.4028/www.scientific.net/SSP.106.41

[9] H. Xu, L. Gao, J. Guo. Preparation and characterizations of tetragonal barium titanate powders by hydrothermal method. Journal of the European Ceramic Society 2002; 22:1163-1170.
DOI: 10.1016/S0955-2219(01)00425-3

[10] C. Gomez-Yañez, C. Benitez, H. Balmori-Ramirez. Mechanical activation of the synthesis reaction of $BaTiO_3$ from a mixture of $BaCO_3$ and TiO_2 powders. Ceramics International 2000; 26:271-277.
DOI: 10.1016/S0272-8842(99)00053-X

[11] H.A.M. van Hal, W.A. Groen, S. Maassen, W.C. Keur. Mechanochemical synthesis of $BaTiO_3$, $Bi_{0.5}Na_{0.5}TiO_3$ and $Ba_2NaNb_5O_{15}$ dielectric ceramics. Journal of the European Ceramic Society 2001; 21:1689-1692.
DOI: 10.1016/S0955-2219(01)00095-4

[12] V. Berbenni, A. Marini, G. Bruni. Effect of mechanical milling on solid state formation of $BaTiO_3$ from $BaCO_3$-TiO_2 (rutile mixtures). Thermochimica Acta 2001; 374:151-158.
DOI: 10.1016/S0040-6031(01)00505-6

[13] F. Liu, N.A. Hashim, Y. Liu, M.R.M. Abed, K. Li. Progress in the production and modification of PVDF membranes. Journal of Membrane Science 2011; 375:1-27.
DOI: 10.1016/j.memsci.2011.03.014

[14] R.P. Vijayakumar, D.V. Khakhar, A. Misra. Phase transformation and enhancement of toughness in polyvinylidene fluoride by onium salts. Journal of Polymer Science Part B: Polymer Physics 2011; 49:1339-1344.
DOI: 10.1002/polb.22303

[15] D. Chen, M. Wang, W-D. Zhang, T. Liu. Preparation and characterization of poly(vinylidene fluoride) nanocomposites containing multiwalled carbon nanotubes. Journal of Applied Polymer Science 2009; 113:644-650.
DOI: 10.1002/app.29311

[16] S. Ansari, E.P. Giannelis. Functionalized graphene sheet-poly(vinylidene fluoride) conductive nanocomposites. Journal of Polymer Science: Part B: Polymer Physics 2009; 47:888-897.
DOI: 10.1002/polb.21695

[17] R.K. Layek, S. Samanta, D.P. Chatterjee, A.K. Nandi. Physical and mechanical properties of poly(methyl methacrylate)-functionalized graphene/poly(vinylidine fluoride) nanocomposites: Piezoelectric β polymorph formation. Polymer 2010; 51:5846-5866.
DOI: 10.1016/j.polymer.2010.09.067

[18] S. Manna, S.K. Batabyal. A.K. Nandi. Preparation and characterization of silver-poly(vinylidene fluoride) nanocomposites: Formation of piezoelectric polymorph of poly(vinylidene fluoride). Journal of Physical Chemistry B 2006; 110:12318-12326.
DOI: 10.1021/jp061445y

[19] V. Sencadas, R. Gregorio Jr, S. Lanceros-Méndez. α to β phase transformation and microstructural changes of PVDF films induced by uniaxial stretch. Journal of Macromolecular Science Part B Physics 2009; 48:514-525.
DOI: 10.1080/00222340902837527.

[20] R.P. Vijayakumar, D.V. Khakhar, A. Misra. Studies on α to β phase transformations in mechanically deformed PVDF Films. Journal of Applied Polymer Science 2010; 117:3491-3497.
DOI: 10.1002/app.32218

[21] S. Satapathy, S. Pawar, P.K. Gupta, K.B.R. Varma. Effect of annealing on phase transition in poly(vinylidene fluoride) films prepared using polar solvent. Bulletin of Materials Science 2011; 34:727-733.
DOI: 10.1007/s12034-011-0187-0

[22] Y.C. Li, S.C. Tjong, R.K.Y. Li. Dielectric properties of binary polyvinylidene fluoride/barium titanate nanocomposites and their nanographite doped hybrids. eXPRESS Polymer Letters 2011; 5:526-534.
DOI: 10.3144/expresspolymlett.2011.51

[23] Y.P. Mao, S.Y. Mao, Z.-G. Ye, Z.X. Xie, L.S. Zheng. Size-dependences of the dielectric and ferroelectric properties of $BaTiO_3$/polyvinylidene fluoride nanocomposites. Journal of Applied Physics 2010; 108:1-6.
DOI: 10.1063/1.3443582

[24] K. Yu, H. Wang, Y. Zhou, Y. Bai, Y. Niu. Enhanced dielectric properties of $BaTiO_3$/poly(vinylidene fluoride) nanocomposites for energy storage applications. Journal of Applied Physics 2013; 113:1-5.
DOI: 10.1063/1.4776740

[25] Z.-M. Dang, H.-Y. Wang, Y.-H. Zhang, J-Q. Qi. Morphology and dielectric property of homogenous $BaTiO_3$/PVDF nanocomposites prepared via the natural adsorption action of nanosized $BaTiO_3$. Macromolecular Rapid Communications 2005; 26:1185-1189.
DOI: 10.1002/marc.200500137

[26] J. Sheth, D. Kumar. Silicon carbide-induced piezoelectric β-phase in poly(vinylidene fluoride) and its properties. Journal of Materials Research 2012; 27:1838-1845.
DOI: 10.1557/jmr.2012.117

[27] Q. Wang, S. Jiang, Y. Zhang, G. Zhang, L. Xiong. Microstructure and morphology in the PVDF films doped with $BiCl_3$. Polymer Bulletin 2011; 66:821-830.

DOI: 10.1007/s00289-010-0383-X

[28] R. Gonçalves, A.C. Lopes, G. Botelho, I.C. Neves, S. Lanceros-Mendez. Influence of solvent properties on the electrical response of poly(vinylidene fluoride)/NaY composites. Journal of Polymer Research 2013; 20:1-8.
DOI: 10.1007/s10965-013-0143-3

[29] T.U. Patro, M.V. Mhalgi, D.V. Khakhar, A. Misra. Studies on poly(vinylidene fluoride) clay nanocomposites: Effect of different clay modifiers. Polymer 2008; 49:3486-3499.
DOI: 10.1016/j.polymer.2008.05.034

[30] J.-W. Kim, W.-J. Cho, C.-S. Ha. Morphology, crystalline structure, and properties of poly(vinylidene fluoride)/silica hybrid composites. Journal of Polymer Science: Part B: Polymer Physics 2002; 40:19-30.
DOI: 10.1002/polb.10071

[31] C. Liao, J. Zhao, P. Yu, H. Tong, Y. Luo. Synthesis and characterization of low content of different SiO_2 materials composite poly(vinylidene fluoride) ultrafiltration membranes. Desalination 2010; 260:147-152.
DOI: 10.1016/j.desal.2011.09.042

[32] R. Song, D. Yang, L. He. Effect of surface modification of nanosilica on crystallization, thermal and mechanical properties of poly(vinylidene fluoride). Journal of Materials Science 2007; 42:8408-8417.
DOI: 10.1007/s10853-007-1787-3

[33] J. Arranz-Andrés, N. Pulido-González, P. Marín, A.M. Aragón, M.L. Cerrada. Electromagnetic shielding features in lightweight PVDF-aluminum based nanocomposites. Progress in Electromagnetics Research B 2013; 48:175-196.
DOI: 10.2528/PIERB12121109

[34] Y.Y. Zhang, S.L. Jiang, Y. Yu, G. Xiong, Q.F. Zhang, G.Z. Guang. Phase transformation mechanisms and piezoelectric properties of poly(vinylidene fluoride)/montmorillonite composite. Journal of Applied Polymer Science 2012; 123:2595-2600.
DOI: 10.1002/app.34431

[35] L. Priya, J.P. Jog. Poly(vinylidene fluoride)/clay nanocomposites prepared by melt intercalation: Crystallization and dynamic mechanical behavior studies. Journal of Polymer Science: Part B: Polymer Physics 2002; 40:1682-1689.
DOI: 10.1002/polb.10223

[36] C.-W. Tang, B. Li, L. Sun, B. Lively, W.-H. Zhong. The effects of nanofillers, stretching and recrystallization on microstructure, phase transformation and dielectric properties in PVDF nanocomposites. European Polymer Journal 2012; 48:1062-1072.
DOI: 10.1016/j.eurpolymj.2012.04.002

[37] I.-H. Kim, D.H. Baik, Y.G. Jeong. Structures, electrical, and dielectric properties of PVDF-based nanocomposite films reinforced with neat multi-walled carbon nanotube. Macromolecular Research 2012; 20:920-927.
DOI: 10.1007/s13233-012-0064-8

[38] J. Yu, P. Jiang, C. Wu, L. Wang, X. Wu. Graphene nanocomposites based on poly(vinylidene fluoride): Structure and properties. Polymer Composites 2011; 32:1483-1491.
DOI: 10.1002/pc.21106

[39] K.P. Pramoda, A. Mohamed, I.Y. Phang, T. Liu. Crystal transformation and thermomechanical properties of poly(vinylidene fluoride)/clay nanocomposites. Polymer International 2005; 54:226-232.
DOI: 10.1002/pi.1692

[40] Q. Zhang, R. Adebisi, J. Gladden. Synthesize procedures, mechanical and electrical properties of poly(vinylidene fluoride) nanocomposite thin films containing multiwalled carbon nanotubes. Polymer Composites 2012; 33:509-514.
DOI: 10.1002/pc.22138

[41] L. Jian, C. Chilan. The preparation and tribological properties of PVDF/TiO_2 nanocomposites. Polymer-Plastics Technology and Engineering 2010; 49:643-647.
DOI: 10.1080/03602551003664636

[42] P. Thomas, S. Satapathy, K. Dwarakanath, K.B.R. Varma. Dielectric properties of poly(vinylidene fluoride)/$CaCu_3Ti_4O_{12}$ nanocrystal composite thick films. eXPRESS Polymer Letters 2010; 4:632-643.
DOI: 10.3144/expresspolymlett.2010.78

[43] S.A.C. Carabineiro, M.F.R. Pereira, J.N. Pereira, C. Caparros, V. Sencadas, S. Lanceros-Mendes. Effect of the carbon nanotube surface characteristics on the conductivity and dielectric constant of carbon nanotube/poly(vinylidene fluoride) composites. Nanoscale Research Letters 2011; 6:1-5.
DOI: 10.1186/1556-276X-6-302

[44] Y. Zhang, S. Jiang, M. Fan, Y. Zeng, Y. Yu, J. He. Piezoelectric formation mechanisms and phase transformation of poly(vinylidene fluoride)/graphite nanosheets nanocomposites. Journal of Materials Science: Materials in Electronics 2013; 24:927-932.
DOI: 10.1007/s10854-012-0851-1

[45] X. Ma, B. Zhou, Y. Deng, Y. Sheng, C. Wang, Y. Pan, Z. Wang. Study on $CaCO_3$/PMMA nanocomposite microspheres by soapless emulsion polymerization. Colloids and Surfaces A: Physicochemical Engineering Aspects 2008; 312:190-194.
DOI: 10.1016/j.colsurfa.2007.06.058

[46] T. Kashiwagi, A. Inaba, J.E. Brown, K. Hatada, T. Kitayama, E. Masuda. Effects of weak linkages on the thermal and oxidative degradation of poly(methy1 methacrylates). Macromolecules 1986; 19:2160-2168.
DOI: 10.1021/ma00162a010

[47] L.E. Manring. Thermal degradation of poly(methy1 methacrylate). 4. Random side-group scission. Macromolecules 1991; 24:3304-3309.
DOI: 10.1021/ma00011a040

[48] T. Kashiwagi, A. Inabil. Behavior of primary radicals during thermal degradation of poly(methyl methacrylate). Polymer Degradation and Stability 1989; 26:161-184.
DOI: 10.1016/0141-3910(89)90007-4

[49] M.C. Costache, D. Wang, M.J. Heidecker, E. Manias, C.A. Wilkie. The thermal degradation of poly(methyl methacrylate) nanocomposites with montmorillonite, layered double hydroxides and carbon nanotubes. Polymers for Advanced Technologies 2006; 17:272-280.
DOI: 10.1002/pat.697

[50] Y.-H. Hu, C.-Y. Chen. Study of the thermal behaviour of poly(methyl methacrylate) initiated by lactams and thiols. Polymer Degradation and Stability 2003; 80:1-10.
DOI: 10.1016/S0141-3910(02)00375-0

[51] K. Brandt, C. Neusel, S. Behr, G.A. Schneider. Dielectric behaviour and conductivity of high-filled $BaTiO_3$-PMMA composites and the facile route of emulsion polymerization in synthesizing the same. Journal of Materials Chemistry C 2013; 1:3129-3137.
DOI: 10.1039/C3TC30204K

[52] L. Xie, X. Huang, C. Wu, P. Jiang. Core-shell structured poly(methyl methacrylate)/$BaTiO_3$ nanocomposites prepared by in situ atom transfer radical

polymerization: a route to high dielectric constant materials with the inherent low loss of the base polymer. Journal of Materials Chemistry C 2011; 21:5897-5906.
DOI: 10.1039/c0jm04574h

[53] A. Laachachi, M. Ferriol, M. Cochez, D. Ruch, J.-M. Lopez-Cuesta. The catalytic role of oxide in the thermooxidative degradation of poly(methyl methacrylate)-TiO_2 nanocomposites. Polymer Degradation and Stability 2008; 93:1131-1137.
DOI: 10.1016/j.polymdegradstab.2008.03.006

[54] S. Ahmad, S. Ahmad, S.A. Agnihotry. Synthesis and characterization of *in situ* prepared poly(methyl methacrylate) nanocomposites. Bulletin of Materials Science 2007; 30:31-35.
DOI: 10.1007/s12034-007-0006-9

[55] B. Hojjati, P.A. Charpentier. Synthesis and kinetics of graft polymerization of methyl methacrylate from the raft coordinated surface of nano-TiO_2. Journal of Polymer Science: Part A: Polymer Chemistry 2008; 46:3926-3937.
DOI: 10.1002/pola.22724

[56] M. Inkyo, Y. Tokunaga, T. Tahara, T. Iwaki, F. Iskandar, C.J. Hogan Jr, K. Okuyama. Beads mill-assisted synthesis of polymethyl methacrylate (PMMA)-TiO_2 nanoparticle composites. Industrial and Engineering Chemistry Research 2008; 47:2597-2604.
DOI: 10.1021/ie071069j

[57] T.E. Motaung, A.S. Luyt, F. Bondioli, M. Messori, M.L. Saladino, A. Spinella, G. Nasillo, E. Caponetti. PMMA-titania nanocomposites: Properties and thermal degradation behaviour. Polymer Degradation and Stability 2012; 97:1325-1333.
DOI: 10.1016/j.polymdegradstab.2012.05.022

[58] J.M. Hwu, G.J. Jiang, Z.M. Gao, W. Xie, W.P. Pan. The characterization of organic modified clay and clay-filled PMMA nanocomposite. Journal of Applied Polymer Science 2002; 83:1702-1710.
DOI: 10.1002/app.10093

[59] L. Martin, G. Kortaberria, A. Vazquez, M. Fermeglia, L. Martinelli, S. Sinesi, A. Jimeno, K. de la Caba, I. Mondragon. A comparative study of nanocomposites based on a recycled poly(methyl methacrylate) matrix containing several nanoclays. Polymer Composites 2008; 29:782-790.
DOI: 10.1002/pc.20438

[60] X. Huang, W.J. Brittain. Synthesis and characterization of PMMA nanocomposites by suspension and emulsion polymerization. Macromolecules 2001; 34:3255-3260.
DOI: 10.1021/ma001670s

[61] K.I. Garcia-Chavez, C.A. Hernandez-Escobar, S.G. Flores-Gallardo, F. Soriano-Corral, E. Saucedo-Salazar, E.A. Zaragoza-Contrerasa. Morphology and thermal properties of clay/PMMA nanocomposites obtained by miniemulsion polymerization. Micron 2013; 49:21-27.
DOI: 10.1016/j.micron.2013.02.007

[62] A. Chatterjee. Properties improvement of PMMA using nano TiO_2. Journal of Applied Polymer Science 2010; 118:2892-2897.
DOI: 10.1002/app.32567

[63] J.-M. Yeh, C.-J.Weng, K.-Y.Huang, H.-Y. Huang, Y.-H Yu. Thermal and optical properties of PMMA-titania hybrid materials prepared by sol-gel approach with HEMA as coupling agent. Journal of Applied Polymer Science 2004; 94:400-405.
DOI: 10.1002/app.20909

[64] S.M. Khaled, R. Sui, P.A. Charpentier, A.S. Rizkalla. Synthesis of TiO_2-PMMA nanocomposite: Using methacrylic acid as a coupling agent. Langmuir2007; 23:3988-3995.
DOI: 10.1021/la062879n

[65] E. Džunuzović, K. Jeremić, J.M. Nedeljković. In situ radical polymerization of methyl methacrylate in a solution of surface modified TiO_2 and nanoparticles. European Polymer Journal 2007; 43:3719-3729.
DOI: 10.1016/j.eurpolymj.2007.06.026

[66] E. Džunuzović, M. Marinović-Cincović, J. Vuković, K. Jeremić, J.M. Nedeljković. Thermal properties of PMMA/TiO_2 nanocomposites prepared by *in-situ* bulk polymerization. Polymer Composites 2009; 30:738-742.
DOI: 10.1002/pc.20606

[67] X. Wang, L. Wu, J. Li. Synergistic flame retarded poly(methyl methacrylate) by nano-ZrO_2 and triphenylphosphate. Journal of Thermal Analysis and Calorimetry 2011; 103:741-746.
DOI: 10.1007/s10973-1050-z

[68] Y. Hu, G. Gu, S. Zhou, L. Wu. Preparation and properties of transparent PMMA/ZrO_2 nanocomposites using 2-hydroxyethyl methacrylate as a coupling agent. Polymer 2011; 52:122-129.
DOI: 10.1016/j.polymer.2010.11020

[69] X. Wang, L. Wu, J. Li. Influence of nanozirconia on the thermal stability of poly(methyl methacrylate) prepared by *in situ* bulk polymerization. Journal of Applied Polymer Science 2010; 117:163-170.
DOI: 10.1002/app.31970

[70] H. Wang, P. Xu, W. Zhong, L. Shen, Q. Du. Transparent poly(methyl methacrylate)/silica/zirconia nanocomposites with excellent thermal stabilities. Polymer Degradation and Stability 2005; 87:319-327.
DOI: 10.1016/j.polymdegradstab.2004.08.015

[71] A. Chatterjee. Effect of nano TiO_2 addition on poly(methyl methacrylate): An exciting nanocomposite. Journal of Applied Polymer Science 2010; 116:3396-3407.
DOI: 10.1002/app.31883

[72] J. Sun, L. Yao, Q.-L. Zhao, J. Huang, R. Song, Z. Ma, L.-H. He, W. Huang, Y.-M Hao. Modification on crystallization of poly(vinylidene fluoride) (PVDF) by solvent extraction of poly(methyl methacrylate) (PMMA) in PVDF/PMMA blends. Frontiers of Materials Science 2011; 5:388-400.
DOI: 10.1007/s11706-011-0152-2

[73] R. Gregorio Jr, N.C. Pereira de Souza Nociti. Effect of PMMA addition on the solution crystallization of the alpha and beta phases of poly(vinylidene fluoride) (PVDF). Journal of Physics D: Applied Physics 1995; 28:432-436.
DOI: 10.1088/0022-3727/28/2/028

[74] I.S. Elashmawi, N.A. Hakeem. Effect of PMMA addition on characterization and morphology of PVDF. Polymer Engineering and Science 2008; 48:895-901.
DOI: 10.1002/pen.21032

[75] H. Song, S. Yang, S. Sun, H. Zhang. Effect of miscibility and crystallization on the mechanical properties and transparency of PVDF/PMMA blends. Polymer-Plastics Technology and Engineering 2013; 52:221-227.
DOI: 10.1080/03602559.2012.735314

[76] M. Li, N. Stingelin, J.J. Michels, M.-J. Spijkman, K. Asadi, K. Feldman, P.W.M. Blom, D.M. de Leeuw. Ferroelectric phase diagram of PVDF:PMMA. Macromolecules 2012; 45:7477-7485.
DOI: 10.1021/ma301460h

[77] W. Li, H. Li, Y-M. Zhang. Preparation and investigation of PVDF/PMMA/TiO_2 composite film. Journal of Materials Science 2009; 44:2977-2984.
DOI: 10.1007/s10853-009-3395-x

[78] J.G. Lee, S.H. Kim, H.C. Kang, S.H. Park. Effect of TiO_2 on PVDF/PMMA composite films prepared by thermal casting. Macromolecular Research 2013; 21:349-355.
DOI: 10.1007/s13233-013-1017-6

[79] W. Ma, S. Chen, J. Zhang, X. Wang. Crystallization behavior and hydrophilicity of poly(vinylidene fluoride) (PVDF)/poly(methylmethacrylate) (PMMA)/poly(styrene-co-acrylonitrile) (SAN) ternary blends. Colloid and Polymer Science 2009; 287:147-155.
DOI: 10.1007/s00396-008-1958-z

[80] G. Wu, T. Miura, S. Asai, M. Sumita. Carbon black-loading induced phase fluctuations in PVDF/PMMA miscible blends: Dynamic percolation measurements. Polymer 2001; 42:3271-3279.
DOI: 10.1016/S0032-3861(00)00417-1

[81] Z. Jin, K.P. Pramoda, S.H. Goh, G. Xu. Poly(vinylidene fluoride)-assisted melt-blending of multi-walled carbon nanotube/poly(methyl methacrylate) composites. Materials Research Bulletin 2002; 37:271-278.
DOI: 10.1016/S0025-5408(01)00775-9

CHAPTER 3

MATERIALS AND METHODS

3.1 Materials

3.1.1 Poly(vinylidene fluoride) (PVDF)

PVDF was supplied in powder form by Solvay Solexis, Brussels (Belgium). It has a melt flow index (MFI) of 0.7 g/10 min (230 °C, 10 kg), a melting point of 173 °C, and a density of 1.78 g cm^{-3}.

3.1.2 Poly(methyl methacrylate) (PMMA)

Commercial grade poly(methyl methacrylate) (PMMA, Altuglas® V920T) produced by Bayer Materials Science, Italy was used. It has a melt flow index (MFI) of 1 g/10 min (230 °C, 3.8 kg) and M_w = 350 000.

3.1.3 Barium titanate ($BaTiO_3$)

$BaTiO_3$ powder (p.a. 99.9%) was supplied by Aldrich *via* the University of Belgrade, Serbia. It was mechanically activated for 0, 5 and 10 min respectively in a planetary ball mill (Fritsch Pulverisette 5) with a zirconia jar and zirconia balls (10 mm in diameter). The ball/sample mass ratio was 20:1, while the tray and vial rotation speeds were 317 and 396 rpm respectively.

3.2 Sample preparation

Table 3.1 shows the different compositions of PVDF/PMMA/$BaTiO_3$. PVDF and PMMA were first placed in an oven at 80 °C overnight to remove moisture. Desired quantities of PVDF, PVDF/$BaTiO_3$, PVDF/PMMA and PVDF/PMMA/$BaTiO_3$ were prepared by mixing in a beaker using a glass rod. Each mixture was transferred into a Brabender Plastograph 50 ml internal mixer, and mixing was conducted for 15 min at a rotor speed of 50 rpm and 200 °C.

The prepared samples were melt pressed at the same temperature and 50 bar pressure for 10 min to form sheets with dimensions of 10x8x1 mm. The ratio of PVDF to PMMA in the blend and blend composites was kept at 80:20. The formed sheets were placed back into the 10x8x1 mm mold, covered with aluminum foil, and melt pressed under the same conditions. After 10 min, the sheets covered with aluminum foil were plunged quickly in ice water. Five minutes later the aluminum foil was removed and the films dried by wiping with a paper towel. The dried films were then annealed at 80 °C for 24 hours.

Table 3.1 Mass percentages of samples used for preparing the blends and nanocomposites

Sample name	% PVDF	% PMMA	% $BaTiO_3$
PVDF	100	0	0
PMMA	100	0	0
PVDF/$BaTiO_3$(0 min)	96	0	4
PVDF/$BaTiO_3$(5 min)	96	0	4
PVDF/PMMA	80	20	0
PVDF/PMMA/$BaTiO_3$ (0 min)	78.4	19.6	2
PVDF/PMMA/$BaTiO_3$ (0 min)	76.8	19.2	4
PVDF/PMMA/$BaTiO_3$ (0 min)	75.2	18.8	6
PVDF/PMMA/$BaTiO_3$ (5 min)	78.4	19.6	2
PVDF/PMMA/$BaTiO_3$ (5 min)	76.8	19.2	4
PVDF/PMMA/$BaTiO_3$ (5 min)	75.2	18.8	6
PVDF/PMMA/$BaTiO_3$ (10 min)	78.4	19.6	2
PVDF/PMMA/$BaTiO_3$ (10 min)	76.8	19.2	4
PVDF/PMMA/$BaTiO_3$ (10 min)	75.2	18.8	6

3.3 Characterization techniques

3.3.1 Scanning electron microscopy (SEM)

SEM is widely used for studying fracture and failure mechanics, particle size and shape, filler orientation and dispersion in polymer matrices [1]. In SEM, the surface of the polymer is

scanned using an electron beam with the reflected or back-scattered beam of electrons collected and displayed on a cathode ray tube screen. The image represents the surface of the scanned material. Polymer surfaces are overlaid with a conductive coating through sputtering or evaporation prior to examination. Coating with a conductive element like gold ensures that the charge deposited on the sample surface by the electron beam is able to leak away to earth [2,3].

The morphology of the pure matrix polymers, PVDF/$BaTiO_3$ and PVDF/PMMA/$BaTiO_3$ composites was investigated by a TESCAN VEGA 3 scanning electron microscope (SEM). The composite samples were fractured after immersion in liquid nitrogen. They were coated with gold and examined at acceleration voltage of 15 kV.

3.3.2 Fourier transform infrared (FTIR) spectroscopy

FTIR provides information on molecular vibrations. It is used for identifying different functional groups by their vibration modes [4]. In ATR-FTIR spectroscopy, a beam of IR is directed to the sample through a high refractive index crystal at an angle larger than the critical angle so that internal reflectance occurs. The resulting internal reflectance forms an evanescent wave, which extends into the sample. On the other end of the crystal the beam is collected by a detector in which the spectrum is generated [5-7].

The presence of the β-phase in all the samples was investigated using a Perkin Elmer Spectrum 100 FTIR spectrophotometer. The samples were analyzed in an attenuated total reflectance (ATR) detector over a 600-4000 cm^{-1} wavenumber range at a resolution of 8 cm^{-1} over 16 scans.

3.3.3 X-ray diffraction (XRD)

XRD is used whenever it is necessary to know the state of chemical combination of the elements involved or the particular phases in which they are present [8]. Generally, this technique operates by generating a beam of X-rays which are diffracted by crystalline structures into particular directions. The measured intensities and angles of the diffracted beams can be used to form a picture of the crystalline structure of the investigated sample [9].

The crystalline phases of the samples were investigated using a D8 Advance diffractometer (BRUKER AXS, Germany) with PSD Vantec-1 detectors and Cu-K_α radiation (λ = 1.5406 Å), a tube voltage of 40 kV, a current of 40 mA and a V20 variable slit. Samples were scanned in locked coupled mode with 2θ ranges from 0 ° to 60 ° with a step size of 0.04 °.

3.3.4 Raman spectroscopy

Raman spectroscopy is used for investigating the structural properties of materials. During the analysis, Raman spectra are obtained by irradiating a sample with a laser source of visible or infrared monochromatic radiation. During irradiation, the spectrum of the scattered radiation is measured at some angle (usually 90 °) with a suitable spectrometer [10]. Raman scattering and infrared absorption spectra often resemble one another closely for a given molecule. However, for some problems, Raman spectroscopy offers more useful information than infrared spectroscopy [10].

Raman spectroscopy was also used for investigating the presence of the β-phase in selected samples and the effect that mechanical activation of $BaTiO_3$ has on the β-phase crystallization. A fully automated Raman microscope (Horiba Jobin Yvon LabRam ARAMIS) was used for the Raman spectroscopy measurements of selected samples. The incident laser was a He-Ne laser at 633 nm. The data was collected over the Raman shift range of 200 to 3200 cm^{-1} using a count time of 5 seconds with 10 averaging cycles. The samples were measured under a microscope using a 100x objective.

3.3.5 Differential scanning calorimetry (DSC)

DSC is a technique in which the difference in energy inputs into a sample and reference is measured as a function of temperature, or time, while they are subjected to a controlled temperature program. DSC can be used for measuring the glass transition temperature and crystallization kinetics, assessing the degree of crystallinity, and studying the melting behaviour of polymers [11]. There are two types of DSC, namely power-compensated and heat flux DSC. In power-compensated DSC, separate furnaces and heaters are used for heating the sample and reference pan whereas in the heat flux DSC the sample and the reference pan are heated in the same furnace by the same heat source [12].

In this study, DSC analysis was performed using a Perkin Elmer DSC 7 differential scanning calorimeter. The instrument operated under nitrogen atmosphere with nitrogen flowing at a rate of 20 ml min^{-1}. It was calibrated using the onset temperatures of zinc and indium standards, as well as the melting enthalpy of indium. Samples with masses between 5 and 10 mg were sealed in aluminum pans. All the samples were heated from 25 to 210 °C at a rate of 20 °C min^{-1}, cooled to 25 °C at 20 °C min^{-1}, re-heated to 210 °C at 20 °C min^{-1}, and cooled to 25 °C at 100 °C min^{-1}. Each composition was analyzed three times to confirm accuracy. First heating and first cooling were reported. The melting and crystallization temperatures, as well as melting enthalpies, are reported as average values with standard deviations.

3.3.6 Thermogravimetric analysis (TGA)

TGA measures the amount and rate of change in the weight of a material as a function of temperature or time in a controlled atmosphere. During the analysis, the sample is kept in a controlled furnace, the temperature of which is measured by a thermocouple. The balance allows continuous mass determination of the sample as the temperature increases [13,14]. A plot of mass as a function of temperature or time represents the thermogravimetric results. TGA is used for measuring thermal stability, decomposition kinetics, composition, estimated lifetime, oxidative stability, moisture, and volatile contents [13].

The influence of $BaTiO_3$ and PMMA on the thermal stability of PVDF was investigated using a Perkin Elmer STA 6000 Simultaneous Thermal Analyzer. Samples with masses between 20 and 25 mg were heated from 30 to 750 °C at a heating rate of 10 °C min^{-1} and a nitrogen flow rate of 20 ml min^{-1}.

3.3.7 Dynamic mechanical analysis (DMA)

Dynamic mechanical analysis is the measurement of the mechanical response of a material as it is deformed under periodic stress, and it is used for characterizing the viscoelastic properties of polymers. Viscoelasticity is the property of materials that may exhibit the characteristics of both a liquid and a solid. The dynamic mechanical analyser simultaneously measures both elastic properties (modulus) and viscous properties (damping) of a material. Such information is essential for the growing trend of the use of polymers as replacement for metals in

structural applications [15,16]. DMA is used to evaluate storage modulus (E'), loss modulus (E"), and damping coefficient tan δ (E"/E') as a function of time, temperature or frequency.

A Perkin Elmer Diamond DMA in tension mode was used for determining the dynamic mechanical properties of the samples. DMA was used for evaluating the effect of $BaTiO_3$ and PMMA on the glass transition temperature of PVDF. The following settings were used during the analysis:

Frequency	1 Hz
Strain	20 μm
Temperature range	-90 to 110 °C
Temperature program mode	Ramp
Heating rate	3 °C min^{-1}
Preloading force	98 mN
Sample length	20 mm
Sample width	5-5.5 mm
Sample thickness	1.2-1.5 mm

3.3.8 Dielectric properties

Dielectric behaviour refers to the variation of the dielectric constant, loss factors, dielectric loss, alternating current conductivity, and direct current conductivity as a function of frequency, composition, voltage, pressure, and temperature. Due to the high dielectric constant of $BaTiO_3$, the effect of $BaTiO_3$ on the dielectric behaviour of PVDF/PMMA in selected samples was investigated. The samples in the form of discs (D = 13 mm, d = 1 mm) were cut from the middle of the sheets. Electrodes were made on the major faces, using soft graphite. Dielectric spectroscopy measurements were performed on a Hameg 8118 instrument in a frequency range 60 to 180 kHz and a temperature range 175 to 380 K, using Temperature Controller Lake Shore 340. The heating rate was 2 ºC min^{-1}, and the acquisition step was 10 ºC with 1.5 V applied voltage. Conductance (G) and susceptance (B) were measured in the C_p measurement model of the instrument. In this case the AC conductivity (σ_{ac}) can be calculated from Equation 3.1.

$$\sigma_{ac} = \sqrt{B^2 + G^2} \quad (3.1)$$

The loss tangent (tan δ) is calculated from Equation 3.2.

$$\tan\delta = G/B = G/2\pi fC \quad (3.2)$$

where f is frequency and C is the capacity. The capacity is also obtained from Equation 3.3.

$$C = \varepsilon'\varepsilon_o S/d \quad (3.3)$$

where ε' is the real part of dielectric permittivity, ε_o is the vacuum permittivity, and S/d describes the geometry of the samples ($S = \pi D^2/4$).

3.4 References

[1] O. Guise, C. Strom, N. Preschilla. STEM-in-SEM method for morphology analysis of polymer systems. Polymer 2011; 52:1278-1285.
DOI: 10.1016/j.polymer.2011.01.030

[2] C.E. Carraher Jr. Carraher's Polymer Chemistry 8th Edition. CRC Press Taylor & Francis Group, Boca Raton (2011).

[3] B.J. Hunt, M.I. James. Polymer Characteristion. Blackie Academic & Professional, London (1993).

[4] B. Stuart. Infrared Spectroscopy: Fundamentals and Applications. John Wiley &Sons Ltd., Chichester (2004).

[5] B.C. Smith. Fundamentals of Fourier Transform Infrared Spectroscopy. CRC Press, New York (2011).

[6] T. Buffeteau, B. Desbat, D. Eyquem. Attenuated total reflection Fourier transform infrared microspectroscopy: Theory and application to polymer samples. Vibrational Spectroscopy 1996; 11:29-36.

[7] J.D. Schuttlefield, V.H. Grassian. ATR-FTIR spectroscopy in the undergraduate chemistry laboratory. Part I: Fundamentals and examples. Journal of Chemical Education 2008; 85:279-281.

DOI: 10.1021/ed085p279

[8] B.B. Cullity, S.R. Stock. Elements of X-Ray Diffraction 3rd Edition. Pearson Prentice Hall, New Jersey (2001).

[9] Y. Leng. Materials Characterization: Introduction to Microscopic and Spectroscopic Methods. John Wiley and Sons, Singapore (2008).

[10] D.A. Skoog, J.J. Leary. Principles of Instrumental Analysis 4th Edition. Saunders College Publishing, Florida (1992).

[11] J.N. Hay. Applications of thermal analysis of polymers. In: E.L. Charsley, S.B. Warrington. Thermal Analysis-Techniques and Applications. The Royal Society of Chemistry, Leeds (1992).

[12] http://media.johnwiley.com.au/product_data/excerpt/13/14051317/1405131713.pdf (Accessed 29 August 2013)

[13] A. Boudenne, L. Ibos, Y. Candau, S. Thomas. Handbook of Multiphase Polymer Systems. John Wiley & Sons Ltd., Chichester (2011).

[14] B. Wunderlich. Thermal Analysis of Polymeric Materials. Springer, Berlin (2005).

[15] T.R. Crompton. Practical Polymer Analysis. Plenum Publishing Corporation, New York (1993).

[16] J.M.G. Cowie. Polymers: Chemistry & Physics of Modern Materials 2nd Edition. Blackie Academic & Professional, London (1993).

CHAPTER 4

RESULTS AND DISCUSSION

4.1 Morphology of samples

The SEM micrographs of PVDF, the PVDF/PMMA blend and the PVDF/$BaTiO_3$ nanocomposites are shown in Figure 4.1. The fracture surfaces of PVDF and PVDF/PMMA are uniform and smooth, but the micrograph of PVDF/PMMA shows phase separation. In the PVDF/$BaTiO_3$ composites, the $BaTiO_3$ particles are well dispersed and embedded in the PVDF matrix. Both the non-activated and 5 minutes mechanically activated $BaTiO_3$ particles formed small agglomerates in the PVDF matrix. The distribution graph in Figure 4.2 shows that most of the particles in both samples range between 0.1 and 0.2 μm. It is also clear from this graph that mechanical activation did not significantly influence the size distribution of the particles in PVDF.

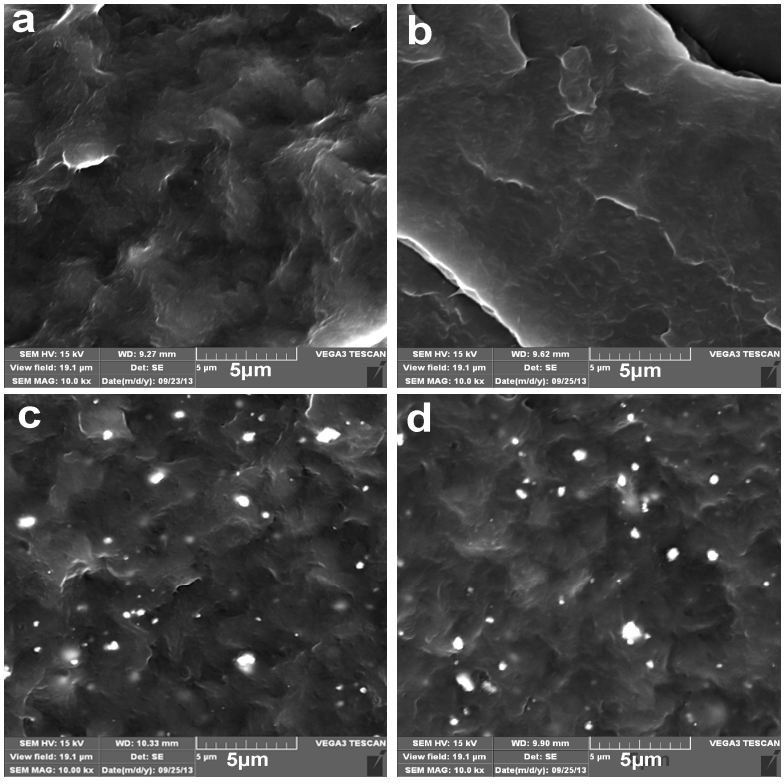

Figure 4.1 SEM micrographs of pure polymer, blend and nanocomposites: (a) PVDF, (b) 80/20 w/w PVDF/PMMA, (c) 96/4 w/w PVDF/$BaTiO_3$ (non-activated), (d) 96/4 w/w PVDF/$BaTiO_3$ (5min activated)

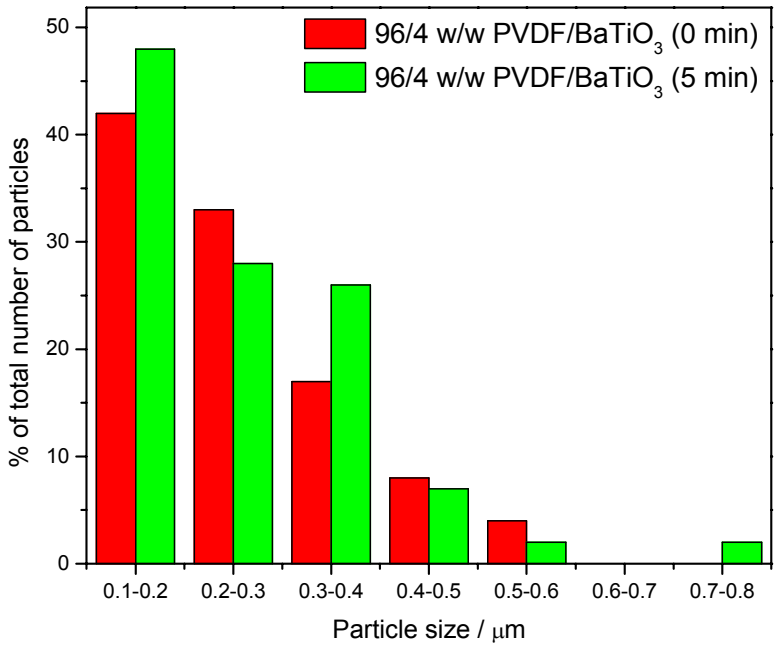

Figure 4.2 Distribution graphs of $BaTiO_3$ particle sizes in PVDF/$BaTiO_3$ composites

The SEM micrographs of the PVDF/PMMA/$BaTiO_3$ nanocomposites are shown in Figures 4.3 to 4.5. The $BaTiO_3$ particles are well dispersed and embedded in the PVDF/PMMA matrix. Nanoparticle agglomerates are also present in these nanocomposites, and the number of agglomerates increases with an increase in $BaTiO_3$ content. It seems like the agglomeration is slightly higher in the case of the non-activated $BaTiO_3$ fillers.

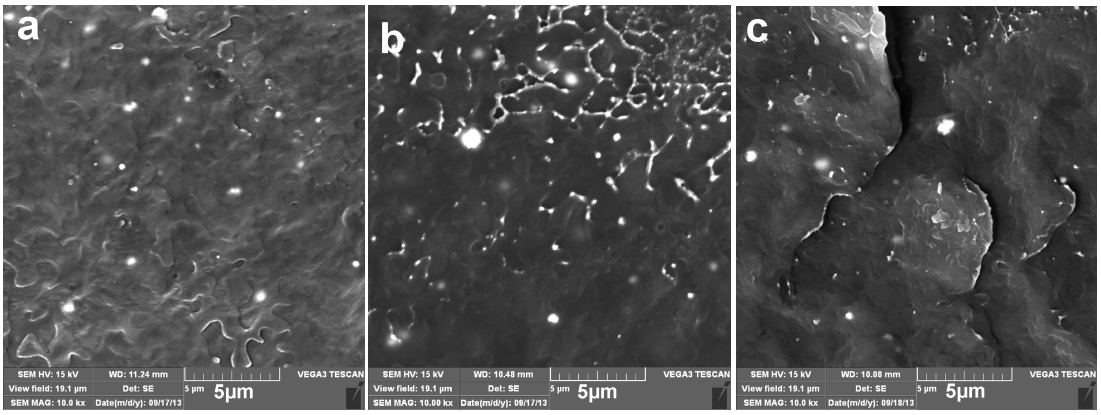

Figure 4.3 SEM micrographs of 78.4/19.6/2.0 w/w PVDF/PMMA/$BaTiO_3$ nanocomposites: (a) non-activated, (b) 5 min activated, (c) 10 min activated

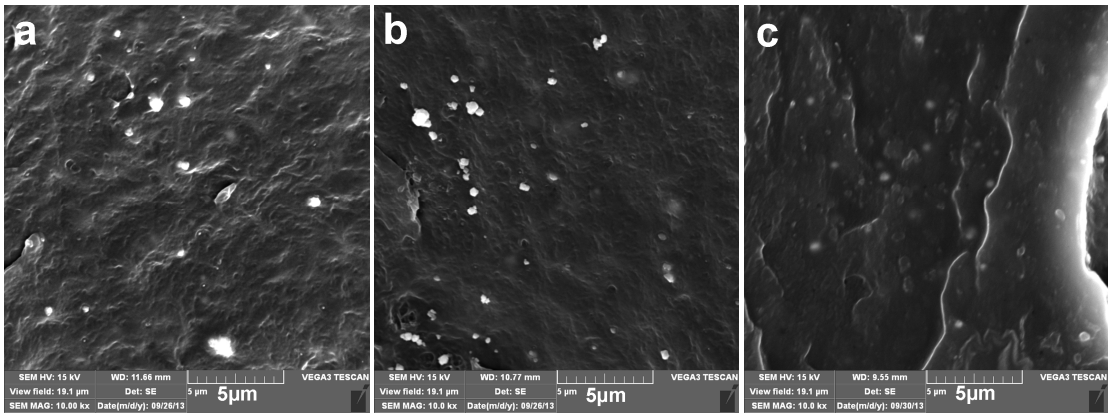

Figure 4.4 SEM micrographs of 76.8/19.2/4.0 w/w PVDF/PMMA/$BaTiO_3$ nanocomposites: (a) non-activated, (b) 5 min activated, (c) 10 min activated

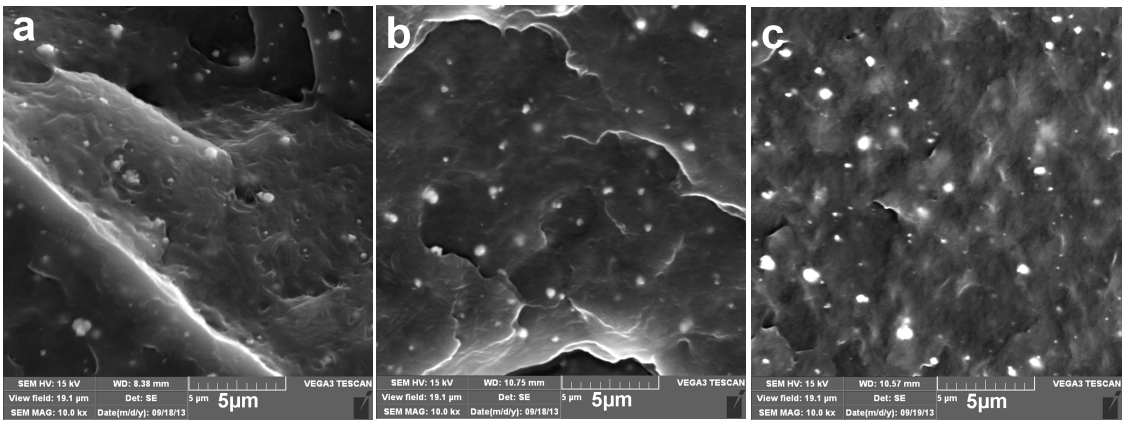

Figure 4.5 SEM micrographs of 75.2/18.8/6.0 w/w PVDF/PMMA/$BaTiO_3$ nanocomposites: (a) non-activated, (b) 5 min activated, (c) 10 min activated

The distribution graphs of the PVDF/PMMA/$BaTiO_3$ nanocomposites are shown in Figures 4.6 to 4.8. It can be seen that the particles with diameters ranging between 0.1 and 0.2µm are dominant in the nanocomposites. Moreover, there are particles with diameters ranging between 0.01 and 0.1 µm in the case of the mechanically activated particles. This is attributed to a breaking up of the agglomerates by the mechanical activation. There are more smaller sized particles in the blend composites for 10 min activated $BaTiO_3$ (Figures 4.6 and 4.8). One would expect to see the same for the samples containing 4 % $BaTiO_3$ (Figure 4.7), but the trend looks different here. The reason for the discrepancy is probably that the SEM photos, used to analyze the size distributions of the filler particles, did not show a statistically representative sample of the particles.

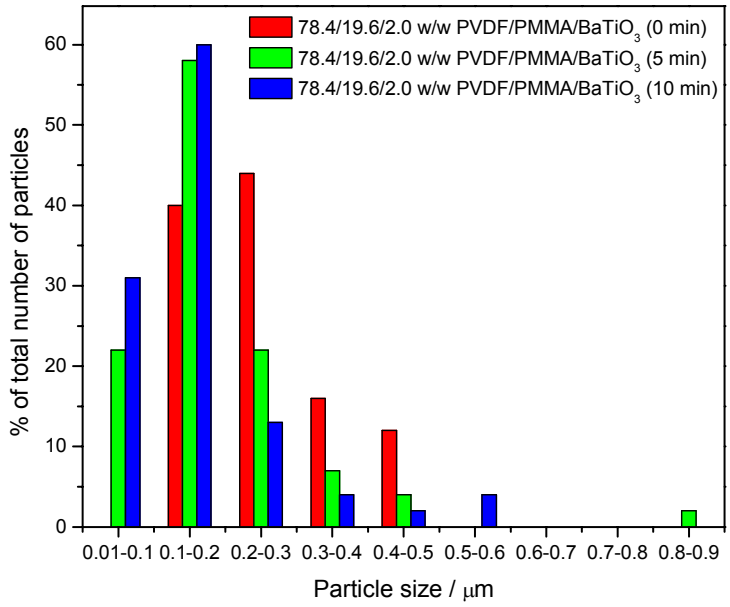

Figure 4.6 Distribution graphs of the $BaTiO_3$ particles in 78.4/19.6/2.0 w/w PVDF/PMMA/$BaTiO_3$

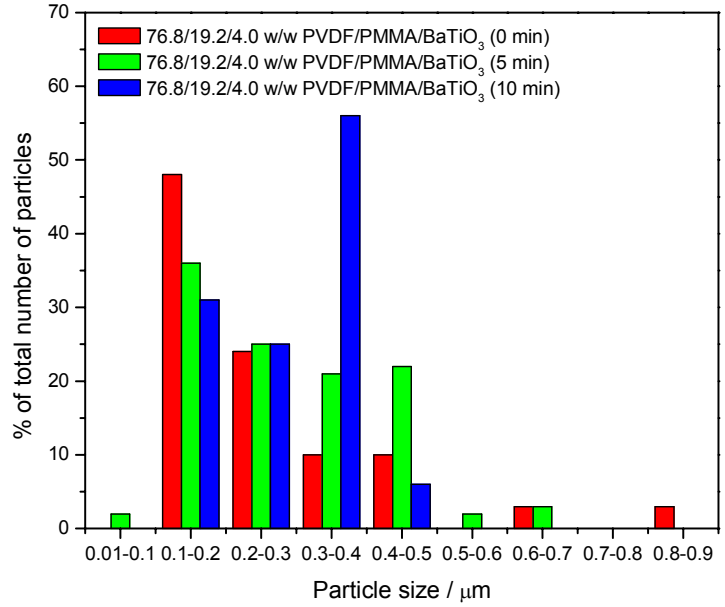

Figure 4.7 Distribution graphs of the $BaTiO_3$ particles in 76.8/19.2/4.0 w/w PVDF/PMMA/$BaTiO_3$

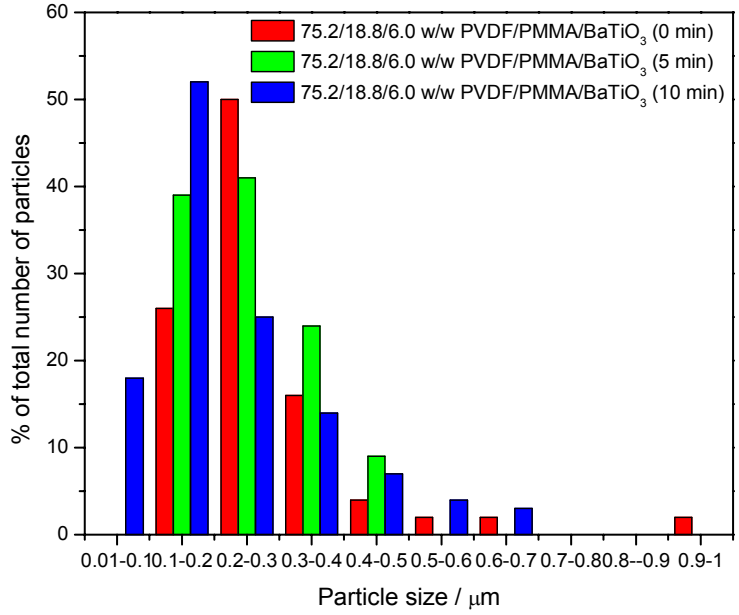

Figure 4.8 Distribution graphs of the $BaTiO_3$ particles in 75.2/18.8/6.0 w/w PVDF/PMMA/$BaTiO_3$

4.2 Fourier transform infrared (FTIR) spectroscopy

The FTIR spectra of all the investigated samples are shown in Figures 4.9 to 4.12. According to previously reported studies [1-4], PVDF has α-phase characteristic peaks at 615, 762, 795, 855, 976, 1150, 1180 and 1384 cm^{-1}. According to Sun *et al*. [5] the γ-phase is represented by peaks at 776, 812 and 833 cm^{-1} [5]. Another study [6] reports the β-phase absorption band at 1278 cm^{-1}, while the absorption band at 842 cm^{-1} represents a combination of the β and γ-phases [6]. The absence of β and γ absorption bands at 842 and 1278 cm^{-1}, and at 776, 812 and 833 cm^{-1}, in the FTIR spectra of PVDF (Figure 4.9) shows that PVDF crystallized exclusively in the α-phase. The addition of non-activated and 5 minutes activated $BaTiO_3$ did not induce β-phase formation in PVDF.

The addition of PMMA to PVDF reduced the intensities of certain α-phase peaks (615, 762, 976 and 1180 cm^{-1}), and new peaks emerged at 1278 and 842 cm^{-1} implying the coexistence of the β- and γ-phases in PVDF/PMMA (Figures 4.10 to 4.12). This result confirms what has

already been known, that blending of PVDF with PMMA is an alternative method to induce β-phase crystallization in PVDF [5]. The presence of the carbonyl stretching peak at 1729 cm^{-1} confirms the presence of PMMA in the blend and the blend composites [7]. The β-phase is also present in the PVDF/PMMA/$BaTiO_3$ nanocomposites as is evident from the peak at 1278 cm^{-1}. It seems as if the 10 minutes mechanically activated $BaTiO_3$ particles interact better with the PVDF/PMMA matrix by inducing more of the β-phase when compared with the non-activated $BaTiO_3$ particles. This is confirmed by the disappearance of the α-phase peaks at 615 and 1150 cm^{-1} in the blend composites with 10 minutes activated $BaTiO_3$, as well as the increase in the intensity of the peaks at 1278 and 842 cm^{-1} (Figure 4.12). This is expected because the 10 minutes mechanically activated $BaTiO_3$ particles have large specific surfaces, which are essential for inducing β-phase crystallization in PVDF. The absence of the γ-phase peaks at 776, 812 and 833 cm^{-1} in PVDF/PMMA and the PVDF/PMMA/$BaTiO_3$ nanocomposites indicates that the β-phase contributes more to the existence of a peak at 842 cm^{-1} than the γ-phase.

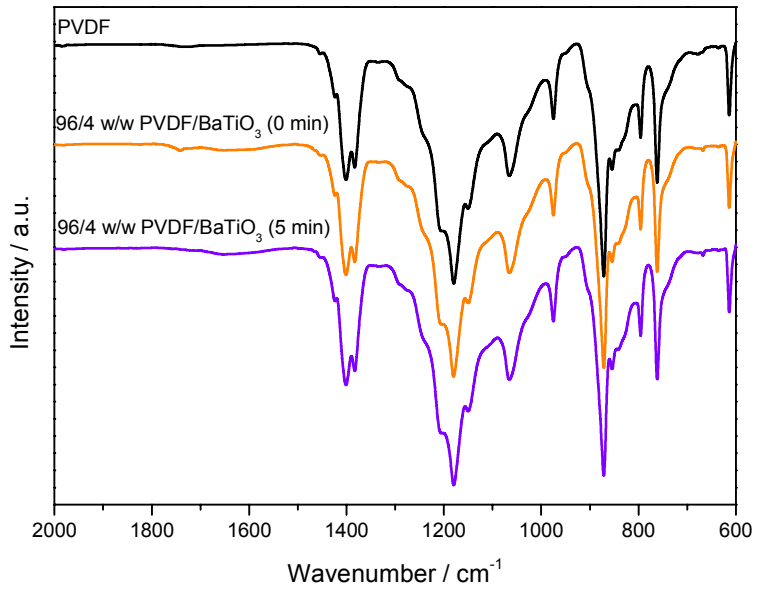

Figure 4.9 FTIR spectra of PVDF and the PVDF/$BaTiO_3$ nanocomposites

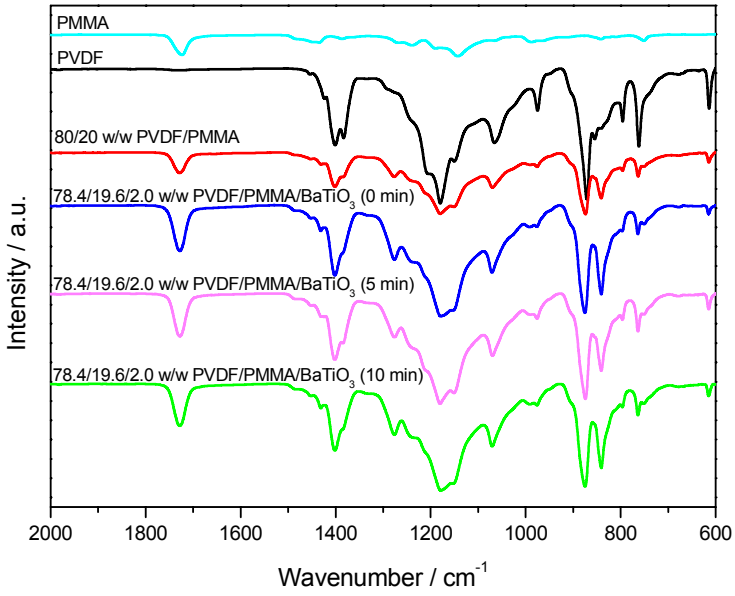

Figure 4.10 FTIR spectra of PMMA, PVDF, PVDF/PMMA and the PVDF/PMMA/$BaTiO_3$ nanocomposites

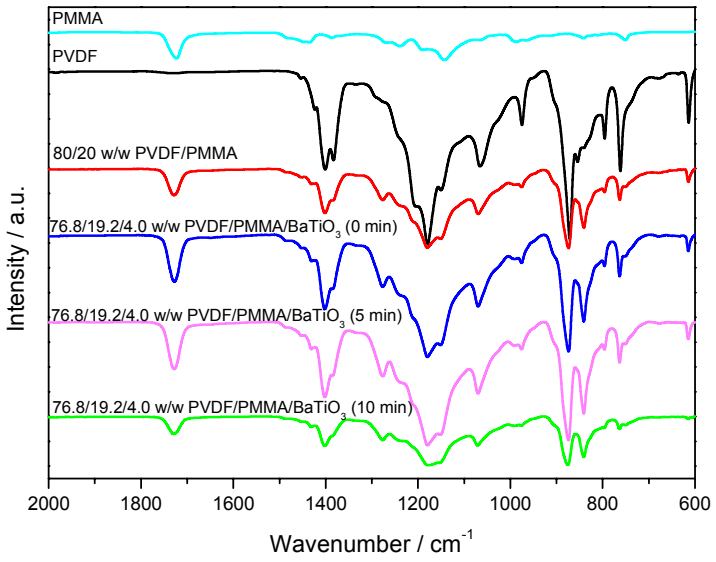

Figure 4.11 FTIR spectra of PMMA, PVDF, PVDF/PMMA and the PVDF/PMMA/$BaTiO_3$ nanocomposites

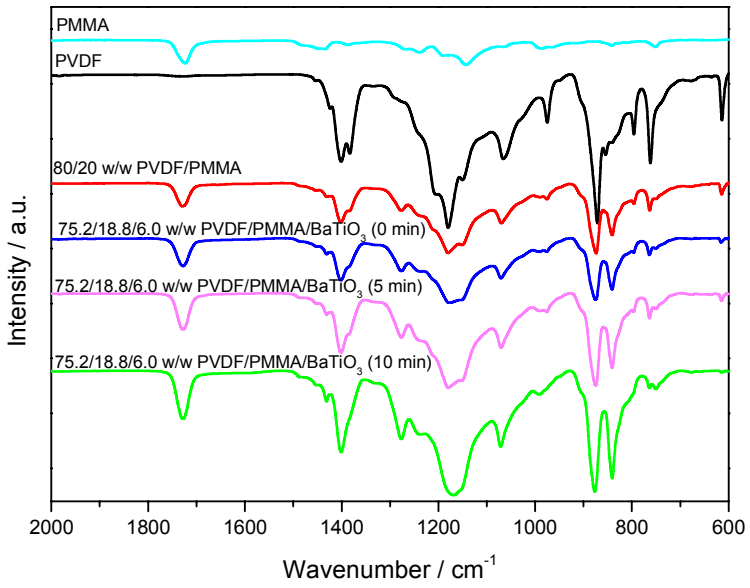

Figure 4.12 FTIR spectra of PMMA, PVDF, PVDF/PMMA and the PVDF/PMMA/$BaTiO_3$ nanocomposites

4.3 X-ray diffractometry

The XRD spectra of all the samples are shown in Figures 4.13 to 4.16. According to previous studies [3,5,6,8], α-phase PVDF has peaks at 2θ= 17.6°, 18.7°, 20°, 21.8°, 26.8° and β-phase PVDF has peaks at 20.3 and 23.5°. It is very challenging for XRD to distinguish between the α- and β-phases in PVDF, because both phases have a common peak around 20° [5,8]. The presence of peaks at 18.7, 19.9, and 26.4° in Figure 4.13 confirms that PVDF crystallized exclusively in the α-phase. The presence of $BaTiO_3$ in PVDF is indicated by peaks at 22.1 and 45.2° [9]. It is clear from Figure 4.13 that the addition of non-activated and 5 minutes activated $BaTiO_3$ did not induce β-phase formation in PVDF. These results are in agreement with the FTIR results.

A new peak in the blend occurred at 20.5° with the addition of PMMA to PVDF (Figures 4.14 to 4.16). This peak is attributed to the presence of the β-phase in PVDF/PMMA. As was

observed in the FTIR results, the intensities of the α-phase peaks at 18.7 and 19.9° decreased with the addition of PMMA. However, it seems like the addition of non-activated $BaTiO_3$ to PVDF/PMMA reduces the intensity of the β-peak at 20.5°, increasing the intensity of the 19.9° α-phase peak in the process. In contrast the intensity of the β-peak at 20.5° increases with the addition of activated fillers. This effect is more observable in the case of the 10 minutes mechanically activated $BaTiO_3$ due to the presence of large specific surfaces which assist in improving the β-phase crystallization.

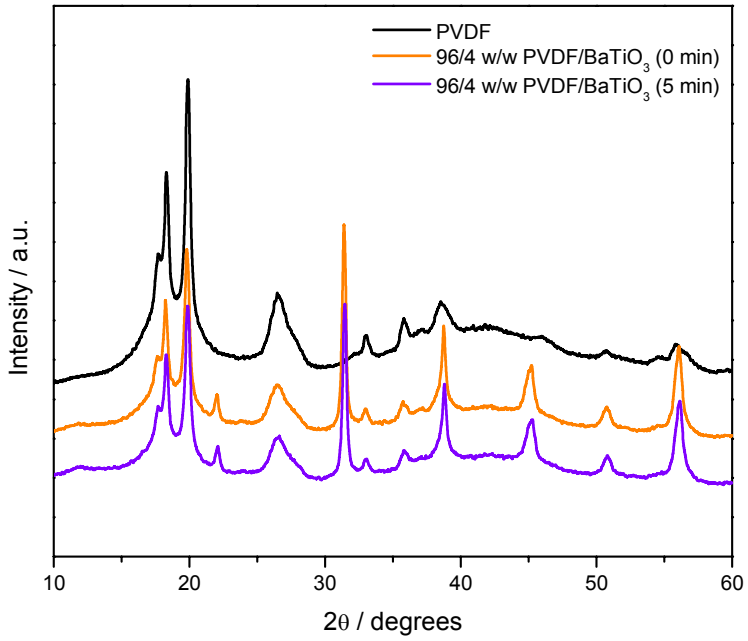

Figure 4.13 XRD spectra of PVDF and the PVDF/$BaTiO_3$ nanocomposites

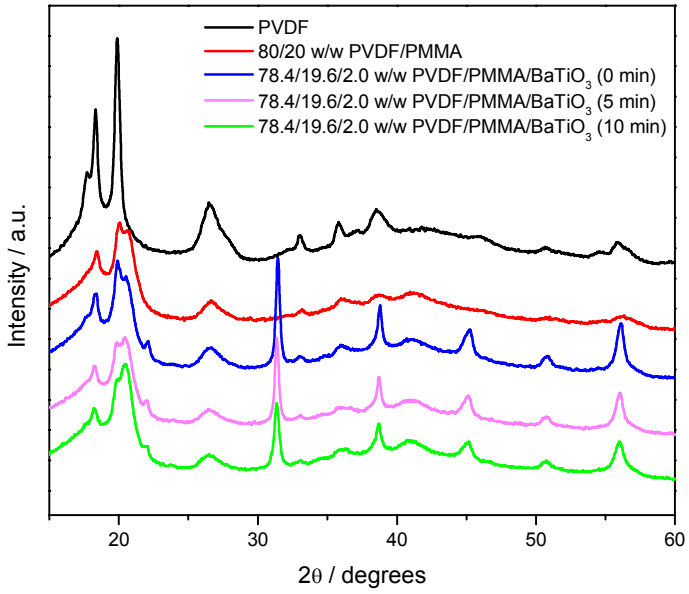

Figure 4.14 XRD spectra of PVDF, PVDF/PMMA and the PVDF/PMMA/$BaTiO_3$ nanocomposites

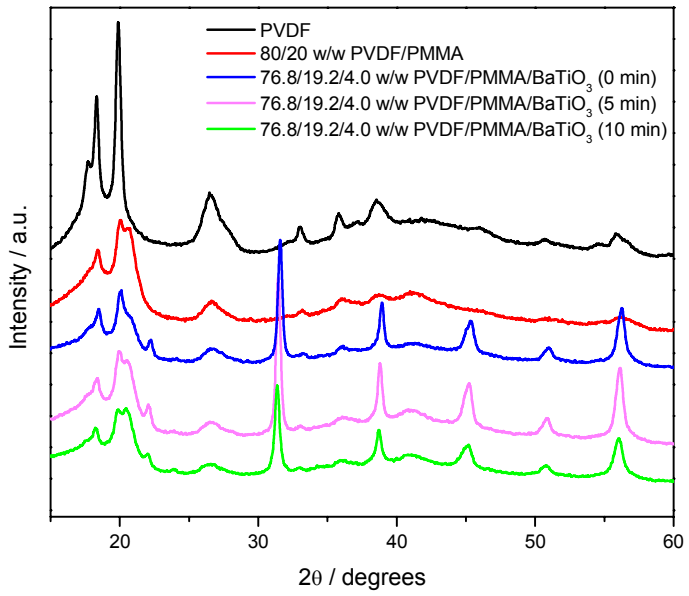

Figure 4.15 XRD spectra of PVDF, PVDF/PMMA and the PVDF/PMMA/$BaTiO_3$ nanocomposites

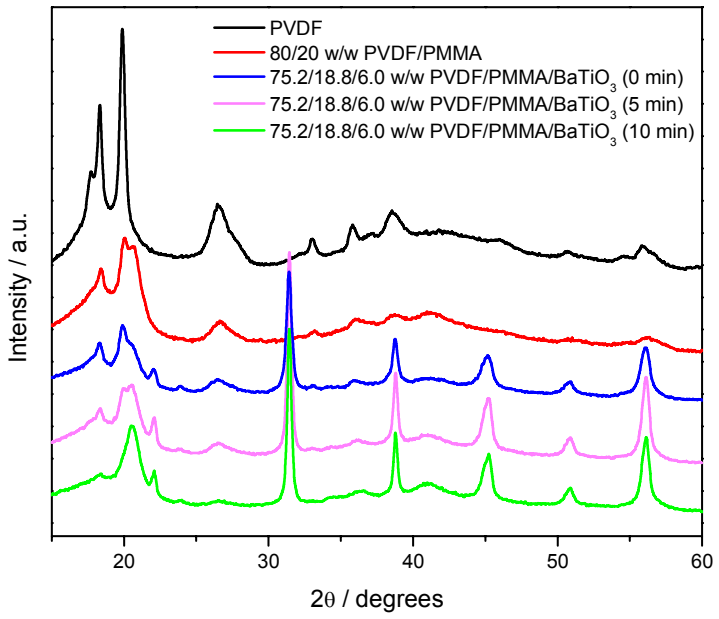

Figure 4.16 XRD spectra of PVDF, PVDF/PMMA and the PVDF/PMMA/$BaTiO_3$ nanocomposites

4.4 Raman spectroscopy

The Raman spectra of the $BaTiO_3$ particles and PMMA are shown in Figure 4.17. The purpose of mechanically activating $BaTiO_3$ was to reduce its size and form large specific surfaces, while maintaining the tetragonal phase. The tetragonal phase is important because it gives $BaTiO_3$ its ferroelectric properties. The presence of peaks at approximately 713, 521, 307 and 260 cm^{-1} in the non-activated and mechanically activated $BaTiO_3$ shows that the nanoparticles have the desired tetragonal phase [10,11]. It is clear that the mechanical activation of the $BaTiO_3$ particles reduced the peak intensities and broadened the peaks. Similar results were observed by Huang *et al.* [12], who showed that the phonon modes at approximately 305 and 720 cm^{-1} ascribed to the tetragonal phase became weak and broad with decreasing size of $BaTiO_3$ particles. They stated that the broadening and weakening of the tetragonal Raman bands suggests that the crystal structure becomes less tetragonal. Moreover, the critical size of $BaTiO_3$ nanoparticles, which is the size of the phase transition from

tetragonal to cubic at room temperature, may be smaller than 30 nm [12]. However, in our case we are of the opinion that the mechanical activation induced a decrease in the particle sizes and at the same time created lattice distortions and a larger number of defects, which caused the broadening and weakening of the Raman bands. Cho *et al.* [13] attributed the peaks at ~260 cm^{-1} and ~306 cm^{-1} to the A1(2TO) and B1 + E(2LO) + E(3TO) modes, respectively, and Qi *et al*. [14] attributed the peaks at ~713 and 521cm^{-1} to the A1(3LO) + E(4LO) and A1(3TO) + E(4TO) modes, respectively. The A1 and E optical modes are separated into transversal (TO) and longitudinal (LO) components due to the long-range electrostatic forces that arise from the ions in the crystal lattice [15]. The Raman bands of tetragonal $BaTiO_3$ particles have been assigned to more than one phonon mode because the wavenumbers of some A1 and E modes are very close, so that the observable modes are mixed.

The phases present and changes occurring in PVDF, PVDF/PMMA and the 76.8/19.2/4.0 w/w PVDF/PMMA/$BaTiO_3$ nanocomposites were obtained by analyzing the Raman spectra in Figure 4.18. The bands in the spectral range between 200 and 1600 cm^{-1} are associated with the presence of α-, β-, and γ-phases. The spectrum of PVDF contains lines at ~811 and 838 cm^{-1} associated with the γ-phase, and a mixture of the β- with γ-phases respectively [16]. The line at ~838 cm^{-1} originates from the CF_2 stretching and CH_2 rocking vibrations. The presence of a peak shoulder at ~796 cm^{-1} (CH_2 rocking) indicates that a small amount of α-phase is present in PVDF [16]. The broad and sharp peaks at ~878 and 1431 cm^{-1} are associated with a mixture of α-, β-, and γ-phases [17]. The peak at ~878 cm^{-1}originates from the C−C asymmetric stretching, while the peak at ~1431 cm^{-1} originates from the CH_2 bending vibrations. The Raman spectrum of PVDF has a peak at ~510 cm^{-1} attributed to both the β- and γ-phases [18]. However, it is evident from the spectra that the γ-phase is dominant in PVDF.

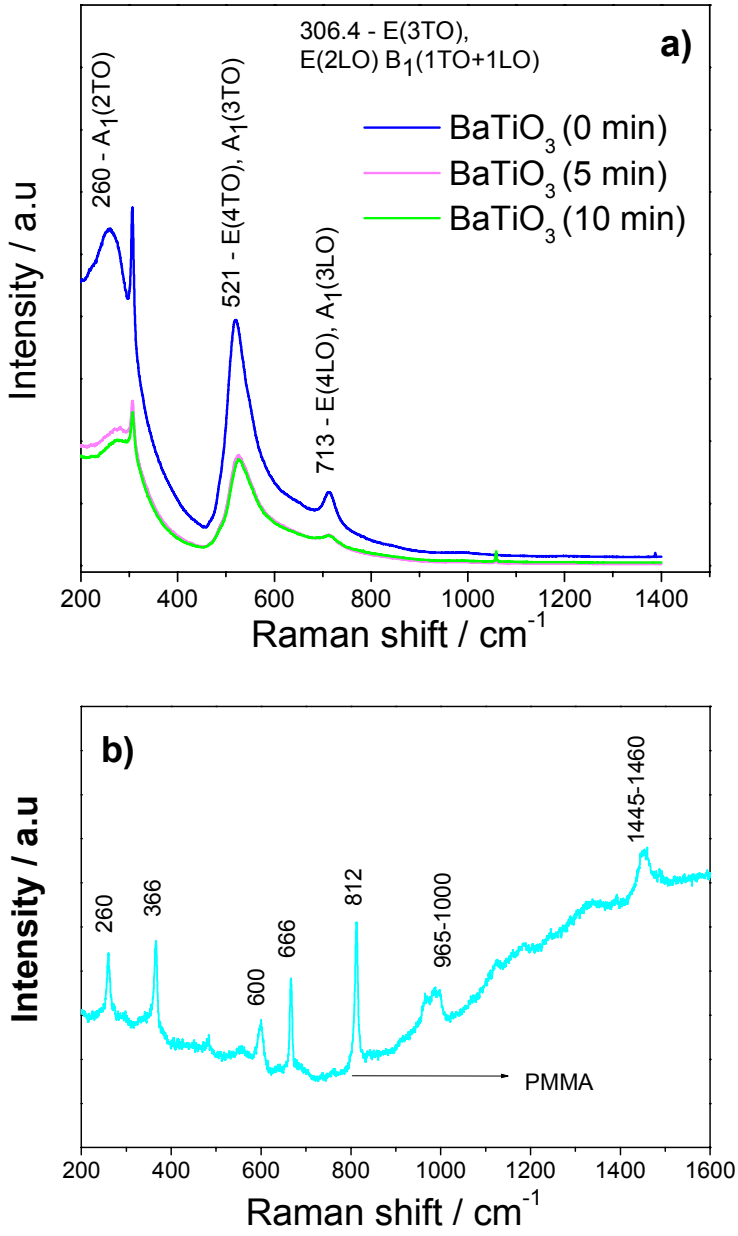

Figure 4.17 Raman spectra of the $BaTiO_3$ nanoparticles and PMMA

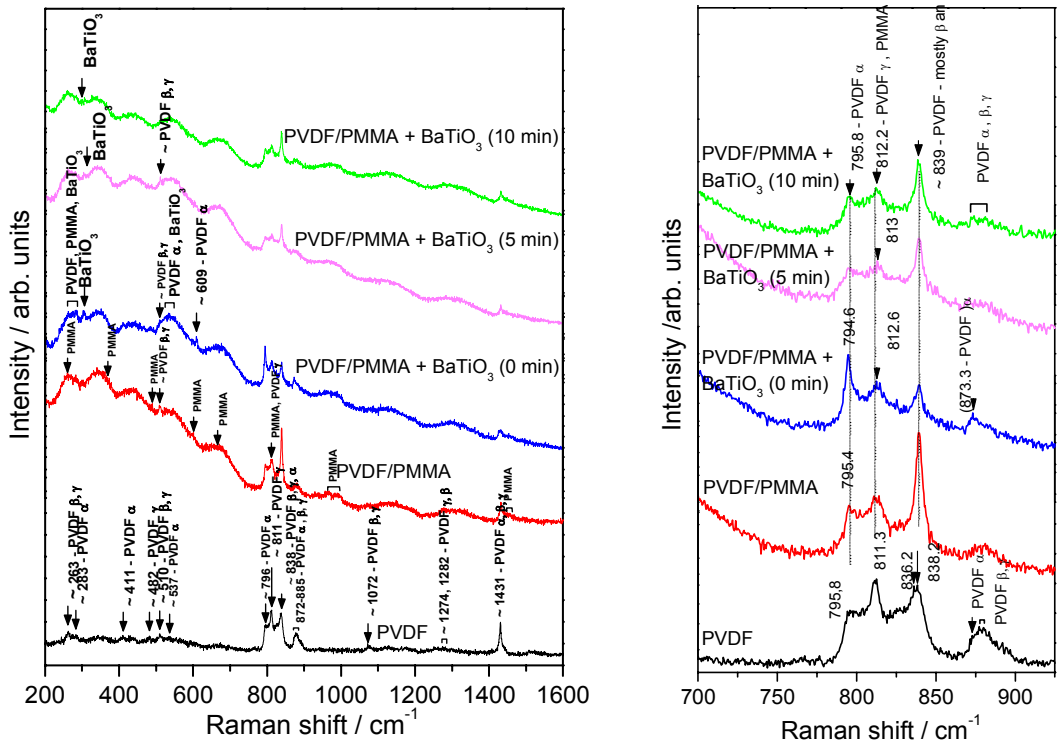

Figure 4.18 Raman spectra of PVDF, PVDF/PMMA and the 76.8/19.2/4.0 w/w PVDF/PMMA/$BaTiO_3$ nanocomposites

The addition of PMMA to PVDF increases the intensity of the peak at ~838 cm^{-1} associated with the β-phase. The intensity of the peak at ~811 cm^{-1}, characteristic of the γ-phase, decreases when PMMA is added. Both PVDF and PMMA contribute to the existence of the peak at ~811 cm^{-1}, because this peak is also observable in the spectra of pure PVDF and pure PMMA. A decrease in the intensity of the peak at ~811 cm^{-1} in the spectrum of PVDF/PMMA suggests that the increase in the intensity of the peak at ~838 cm^{-1} is caused by an increase in the β-phase. For the nanocomposites it seems as if the non-activated and activated fillers affect the crystalline phases of PVDF in different ways. The addition of non-activated $BaTiO_3$ in PVDF/PMMA favours the formation of the α-phase. This is evident from the increase in the intensity of the peak at ~796 cm^{-1} (characteristic of the α-phase), and a decrease in the intensity of the peak at ~838 cm^{-1} (characteristic of the β-phase). Moreover, an α-phase peak, which was not observed in the spectra of PVDF and PVDF/PMMA, emerged at ~609 cm^{-1} (CF_2 wagging and CH_2 twisting vibrations [17]). The intensity of the peak at ~510 cm^{-1} (β- and γ-phases) is reduced when non-activated $BaTiO_3$ is added into the blend. The presence of tetragonal $BaTiO_3$ in the blend nanocomposites is confirmed by the existence of a peak at

~306 cm^{-1}, which is more visible in the nanocomposite containing non-activated $BaTiO_3$. This peak is not easily visible in the nanocomposites with highly activated $BaTiO_3$ due to the broadening of the $BaTiO_3$ peaks caused by mechanical activation. For the blend nanocomposites containing activated $BaTiO_3$, the presence of activated nanoparticles promoted β-phase crystallization in PVDF/PMMA. This is evident from the increase in the intensities of the β-phase peak at ~838 cm^{-1} and the peak at ~510 cm^{-1} associated with both the β- and γ-phases. The intensity of an α-phase peak at ~795 cm^{-1} also decreased when activated $BaTiO_3$ were added. These nanoparticles promoted the β-phase crystallization in PVDF/PMMA due to their smaller size and larger specific surfaces.

4.5 Differential scanning calorimetry (DSC)

The DSC curves of the investigated samples are shown in Figures 4.19 to 4.22. The DSC characteristics of the samples are summarized in Table 4.1. PVDF shows a single melting peak (Figure 4.19) which is associated with the melting of the α-phase crystals observed from FTIR and XRD results. The addition of $BaTiO_3$ to PVDF had no significant influence on the melting temperature of PVDF (Table 4.1). The normalized melting enthalpy of PVDF did not change when $BaTiO_3$ was added, irrespective of the activation time, which indicates that the extent of crystallization was the same.

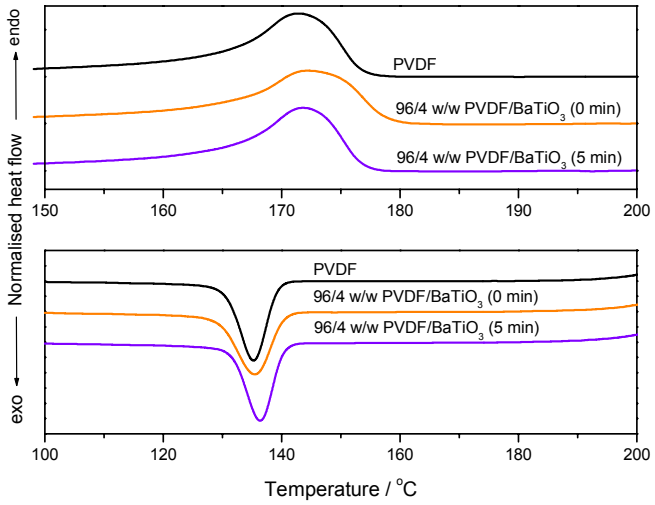

Figure 4.19 Heating and cooling curves of PVDF and the PVDF/$BaTiO_3$ nanocomposites

Table 4.1 DSC melting and crystallization parameters of the investigated samples

Sample	T_c / °C	ΔH_c / Jg^{-1}	ΔH^n_c/ Jg^{-1}	T_m / °C	ΔH_m/ Jg^{-1}	ΔH^n_m/Jg^{-1}
PVDF	135.2 ± 0.2	55.8 ± 4.8	55.8 ± 4.8	171.6 ± 0.4	49.8 ± 1.1	49.8 ± 1.1
96/4 w/w PVDF/$BaTiO_3$ (0 min)	135.6 ± 0.3	57.1 ± 2.6	59.5± 2.7	172.3 ± 0.7	47.5 ± 0.9	49.5 ± 0.9
96/4 w/w PVDF/$BaTiO_3$ (5 min)	136.3 ± 0.6	59.5 ± 2.1	62.0± 2.2	172.5 ± 1.4	47.4 ± 0.9	49.4 ± 0.9
80/20 w/w PVDF/PMMA	125.2 ± 0.8	45.5 ± 2.9	56.9 ± 3.6	170.1 ± 0.7	39.8 ± 2.0	49.8 ±2.5
78.4/19.6/2.0 w/w PVDF/PMMA/$BaTiO_3$(0 min)	125.7 ± 0.2	46.8 ± 3.3	59.7 ± 4.2	169.2 ± 0.2	38.0 ± 0.6	48.5 ± 0.8
78.4/19.6/2.0 w/w PVDF/PMMA/$BaTiO_3$(5 min)	125.9 ± 0.0	45.9 ± 0.6	58.6 ± 0.8	169.6 ± 0.5	37.1 ±1.0	47.3 ± 1.3
78.4/19.6/2.0 w/w PVDF/PMMA/$BaTiO_3$ (10 min)	126.2 ± 0.5	45.3 ± 3.6	57.8 ± 4.6	169.7 ± 0.9	39.9 ± 1.0	50.9 ± 1.3
76.8/19.2/4.0 w/w PVDF/PMMA/$BaTiO_3$(0 min)	126.2 ± 0.5	45.3 ± 3.6	59.0 ± 4.7	169.6 ± 0.4	37.2 ± 1.4	48.4± 1.8
76.8/19.2/4.0 w/w PVDF/PMMA/$BaTiO_3$(5 min)	125.9 ± 0.3	46.8 ± 3.5	60.9 ± 4.6	169.6 ± 0.2	37.7 ± 1.3	49.1± 1.7
76.8/19.2/4.0 w/w PVDF/PMMA/$BaTiO_3$ (10 min)	126.3 ± 0.0	42.5 ± 3.4	55.3 ± 4.4	168.6 ± 0.5	36.1 ± 4.2	47.0± 5.5
75.2/18.8/6.0 w/w PVDF/PMMA/$BaTiO_3$(0 min)	126.4 ± 0.2	44.2 ± 3.7	58.8 ± 4.9	169.4 ± 0.6	39.0 ± 0.9	51.9 ± 1.2
75.2/18.8/6.0 w/w PVDF/PMMA/$BaTiO_3$(5 min)	125.9 ± 0.6	42.7 ± 2.2	56.8 ± 2.9	170.2 ± 1.2	37.5 ± 1.3	49.9± 1.7
75.2/18.8/6.0 w/w PVDF/PMMA/$BaTiO_3$ (10 min)	126.4 ± 0.2	47.4 ± 4.2	63.0 ± 5.6	168.7 ± 0.3	35.8 ± 2.3	47.6 ± 3.1

T_m-melting peak temperature, T_c-crystallization peak temperature, ΔH_m-melting enthalpy, ΔH_c-crystallization enthalpy, ΔH^n_c-crystallization enthalpy normalized with respect to PVDF content, ΔH^n_m-melting enthalpy normalized with respect to PVDF content

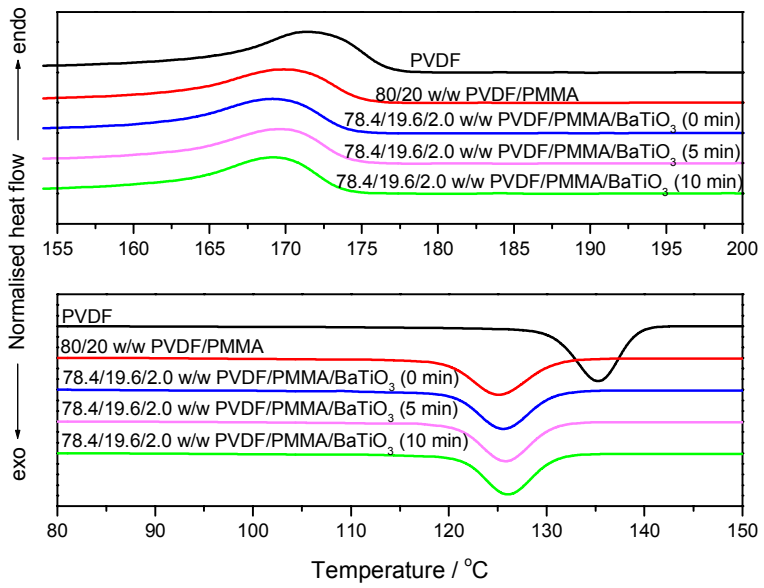

Figure 4.20 Heating and cooling curves of PVDF, PVDF/PMMA and the PVDF/PMMA/$BaTiO_3$ nanocomposites

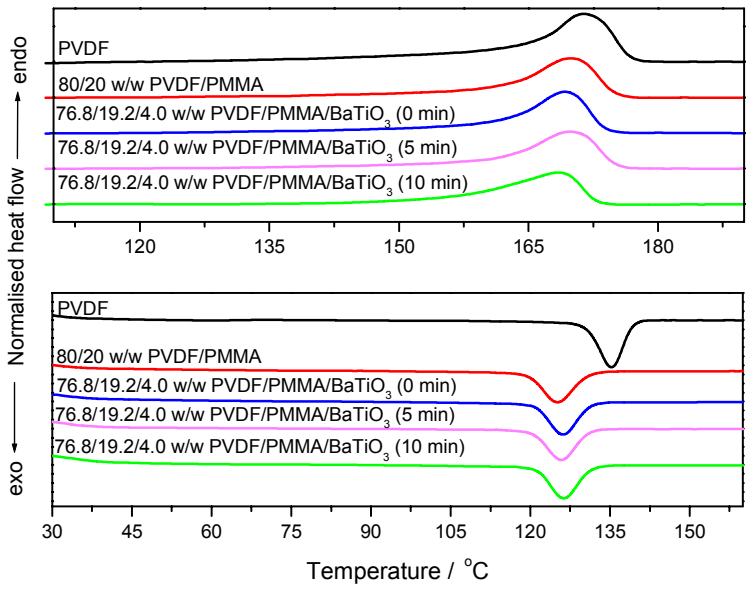

Figure 4.21 Heating and cooling curves of PVDF, PVDF/PMMA and the PVDF/PMMA/$BaTiO_3$ nanocomposites

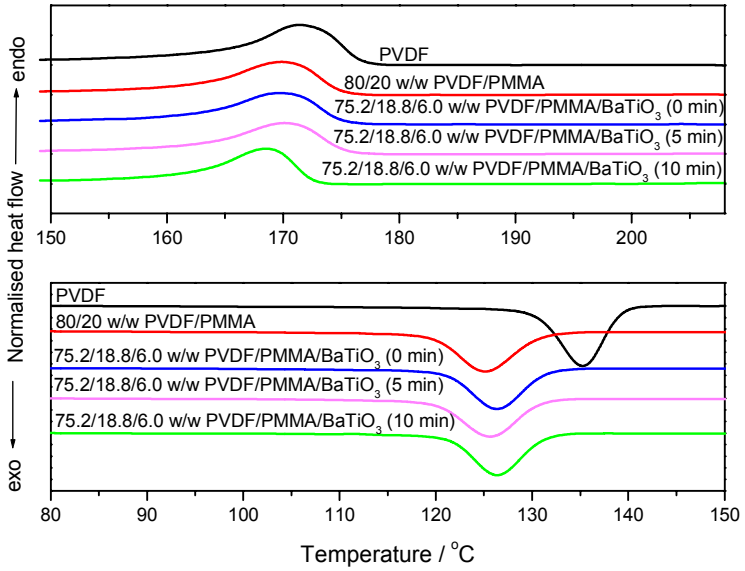

Figure 4.22 Heating and cooling curves of PVDF, PVDF/PMMA and the PVDF/PMMA/$BaTiO_3$ nanocomposites

The melting temperature of PVDF decreased when in the presence of PMMA. This effect was caused by the influence of PMMA on the crystallization process of PVDF, which probably resulted in smaller and more imperfect crystals [1]. The incorporation of $BaTiO_3$ fillers into PVDF/PMMA did not significantly affect the melting temperature of PVDF in PVDF/PMMA. The pure blend and the blend nanocomposites have a single melting peak, irrespective of the crystalline phases present. The single melting peak implies that the melting temperatures of the α- and β-phase crystals are very close to each other [6]. However, there is disagreement in the literature regarding the melting temperatures of the α- and β-phases of PVDF. According to Vijayakumar *et al.* [19] there is a double melting point phenomenon in PVDF showed polymorphism, with the α-phase crystals melting at a lower temperature than the β-phase crystals. Kim *et al*. [20], on the other hand, showed that α-phase PVDF had a single melting peak where the peak temperature decreased as nanofillers were added. They attributed this to the presence of or increase in the β-phase, which was detected by FTIR and XRD. According to them the β-phase crystals melt at lower temperatures than the α-phase crystals, which contradicts Vijayakumar *et al.* [19]. Imamura *et al*. [21] showed that PVDF containing a mixture of α- and β-phase crystals has a single melting peak attributed to the melting of both

phases. As in the case of pure PVDF as matrix, the normalized melting enthalpy of PVDF in the blend and blend nanocomposites showed no significant change when PMMA and $BaTiO_3$ were added.

It is clear from the DSC results discussed above that β-crystal formation does not add to the total crystallinity of PVDF, but that β-crystallization occurs at the expense of α-crystallization.

4.6 Thermogravimetric analysis (TGA)

The thermal degradation curves of the investigated samples are shown in Figures 4.23 to 4.26. A summary of the decomposition temperatures of the samples are tabulated in Table 4.2. It can be seen from Table 4.2 and Figure 4.23 that PVDF higher decomposition temperatures associated with 10 and 50 % mass loss than the PVDF/$BaTiO_3$ composites, indicate a higher thermal stability for PVDF. The $BaTiO_3$ nanoparticles clearly have a catalyzing effect on the degradation of PVDF. Similar results were obtained by Li *et al.* [22], and they mentioned that metal oxide-catalyzed oxidative decomposition pathways in the PVDF/PMMA/TiO_2 composites were the cause for the decrease in thermal stability of PVDF/PMMA. There are no significant differences on the thermal stabilities of PVDF/$BaTiO_3$ (0 min) and PVDF/$BaTiO_3$ (5 min) composites. Figures 4.24 to 4.26 show the thermal degradation curves of the blend nanocomposites. It can be seen in Table 4.2 that PVDF has higher $T_{10\%}$ and $T_{50\%}$ than PMMA, indicating better thermal stability of PVDF due to the high bond dissociation energy of the C—F bonds. The blending of PVDF and PMMA increases $T_{10\%}$, and this suggests that PVDF acted as an effective thermal barrier that retarded the degradation of PMMA. The two step mass loss in the PVDF/PMMA blend, which correlates well with the 8:2 PVDF:PMMA ratio, is the result of the individual degradation of PMMA and PVDF. The addition of the different $BaTiO_3$ fillers into PVDF/PMMA had no noticeable effect on $T_{10\%}$, but decreased $T_{50\%}$. The blend composites containing 2 % $BaTiO_3$ have the same $T_{50\%}$, irrespective of mechanical activation. For 4 and 6 % $BaTiO_3$ the blend composites with 10 minutes mechanically activated $BaTiO_3$ have $T_{50\%}$ values that are slightly higher than those of the samples containing non-activated and 5minutes mechanically activated $BaTiO_3$. This is probably because the $BaTiO_3$ particles in the composites with 6 % 10 min. activated $BaTiO_3$ acted as a

more effective thermal barrier because they were smaller and better dispersed, as was observed from the SEM results.

Table 4.2 Thermal degradation results ($T_{10\%}$: decomposition temperature associated with a 10% mass loss; $T_{50\%}$: decomposition temperature associated with a 50% mass loss) for all the investigated samples

Sample	$T_{10\%}$ / ºC	$T_{50\%}$ / ºC	% Char at 742 ºC
PVDF	467.2	485.4	27.2
96/4 w/w PVDF/$BaTiO_3$ (0 min)	449.3	479.9	31.9
96/4 w/w PVDF/$BaTiO_3$ (5 min)	449.9	479.9	32.4
PMMA	347.9	373.9	0
80/20 w/w PVDF/PMMA	389.3	482.3	21.8
78.4/19.6/2.0 w/w PVDF/PMMA/$BaTiO_3$ (0 min)	389.6	466.6	24.8
78.4/19.6/2.0 w/w PVDF/PMMA/$BaTiO_3$ (5 min)	383.9	464.9	23.9
78.4/19.6/2.0 w/w PVDF/PMMA/$BaTiO_3$ (10 min)	388.8	465.8	24.3
76.8/19.2/4.0 w/w PVDF/PMMA/$BaTiO_3$ (0 min)	390.5	465.5	25.7
76.8/19.2/4.0 w/w PVDF/PMMA/$BaTiO_3$ (5 min)	387.8	469.8	25.2
76.8/19.2/4.0 w/w PVDF/PMMA/$BaTiO_3$ (10 min)	386.8	470.8	25.7
75.2/18.8/6.0 w/w PVDF/PMMA/$BaTiO_3$ (0 min)	392.0	467.0	27.8
75.2/18.8/6.0 w/w PVDF/PMMA/$BaTiO_3$ (5 min)	391.4	467.4	27.9
75.2/18.8/6.0 w/w PVDF/PMMA/$BaTiO_3$ (10 min)	390.7	472.7	27.0

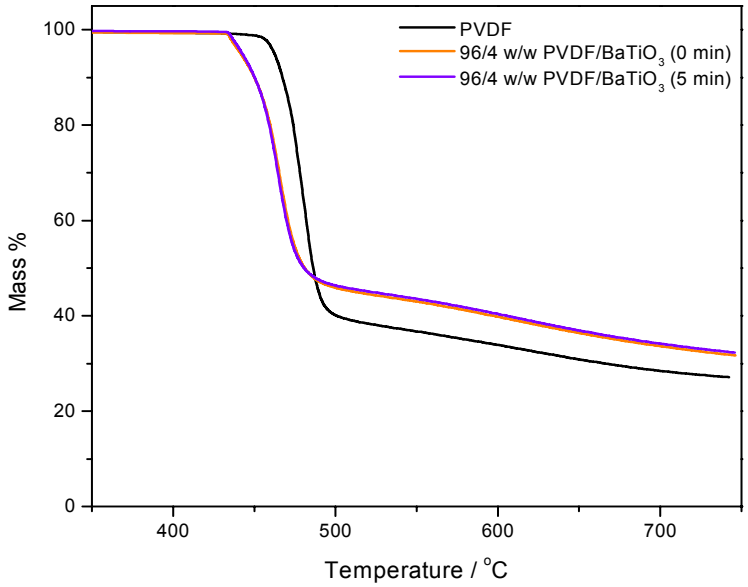

Figure 4.23 TGA curves of PVDF and the PVDF/$BaTiO_3$ nanocomposites

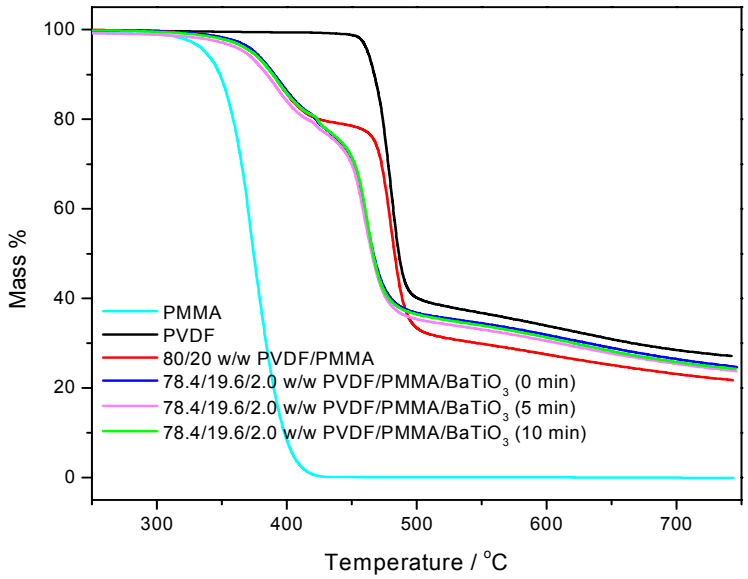

Figure 4.24 TGA curves of PVDF, PMMA, PVDF/PMMA, and the PVDF/PMMA/$BaTiO_3$ nanocomposites

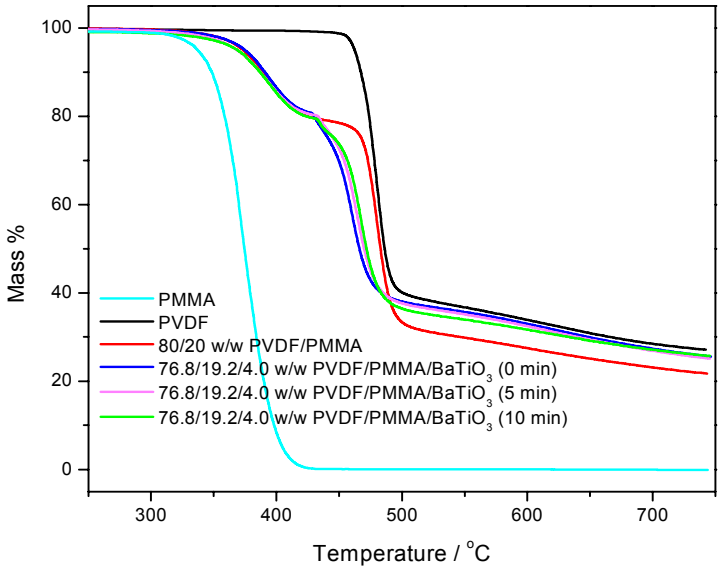

Figure 4.25 TGA curves of PVDF, PMMA, PVDF/PMMA, and PVDF/PMMA/$BaTiO_3$ nanocomposites

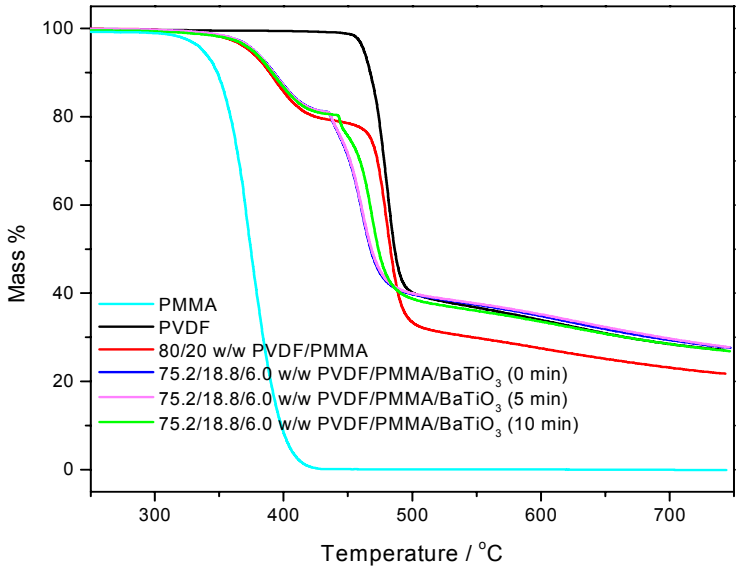

Figure 4.26 TGA curves of PVDF, PMMA, PVDF/PMMA, and the PVDF/PMMA/$BaTiO_3$ nanocomposites

PMMA decomposed completely, while PVDF had a residual char of 27 % at 740 ºC. The addition of PMMA to PVDF decreased the char residue to 22 % at the same temperature. The decrease in the amount of char residue of the blend correlates with the decrease in the amount of PVDF in the blend. Similar results were obtained by Li *et al.* [22]. They attributed the high char residue in PVDF and PVDF/PMMA to the formation of hydrogen fluoride, which introduced unsaturation in the polymer backbone. Moreover, the char content for the blend composites increased proportionally with the amount of $BaTiO_3$ incorporated. This increase is in line with the amount of $BaTiO_3$ in the respective samples, because the filler did not decompose during the heating of the nanocomposites, and it was well dispersed in the polymer blends.

4.7 Dynamic mechanical analysis (DMA)

The influence of non-activated and 5 minutes mechanically activated $BaTiO_3$ nanoparticles on the storage modulus and tan δ of PVDF are shown in Figures 4.27 and 4.28. The loss modulus curves are reported in the appendix. The storages modulus (E') represents the ability of a material to store energy when an oscillatory force is applied, while the loss modulus (E") represents the ability of a material to lose energy when the oscillatory force is applied [23]. The PVDF nanocomposites have higher E' values than pristine PVDF over the whole temperature range. Moreover, the nanocomposites containing mechanically activated $BaTiO_3$ nanoparticles have slightly higher E' values than those containing non-activated $BaTiO_3$ nanoparticles. The higher E' values in PVDF nanocomposites are attributed to the high stiffness of $BaTiO_3$ nanoparticles, which in turn enhances the stiffness of PVDF. The activated $BaTiO_3$ nanoparticles are able to promote more reinforcement in the nanocomposites due to their larger specific surfaces when compared with non-mechanically activated $BaTiO_3$ nanoparticles. This led to stronger interaction with the polymer chains, leading to more immobilization, and consequently resulting in higher E' values.

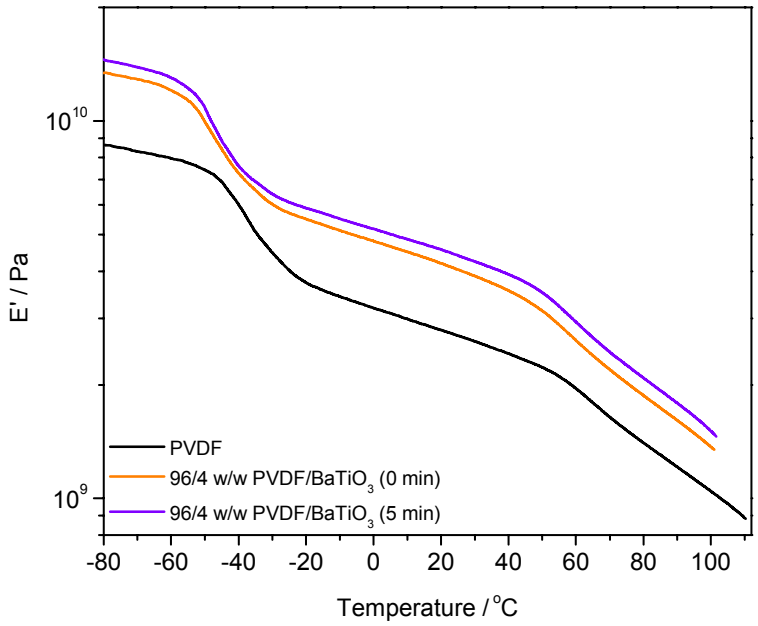

Figure 4.27 Storage modulus as function of temperature of PVDF and the PVDF/$BaTiO_3$ nanocomposites

The tan δ curve of PVDF has relaxations at -34 and 105 °C. The first relaxation is called the α_a-relaxation and it is associated with the segmental motion of the amorphous regions of PVDF, that is the glass transition [24,25]. The relaxation at 105 °C is the α_c-relaxation and is associated with the molecular motion in the crystalline phase [26]. The addition of $BaTiO_3$ to PVDF has no noticeable effect on the α_a- and α_c-relaxation peaks. This means that these nanoparticles have very little influence on the chain mobility of PVDF.

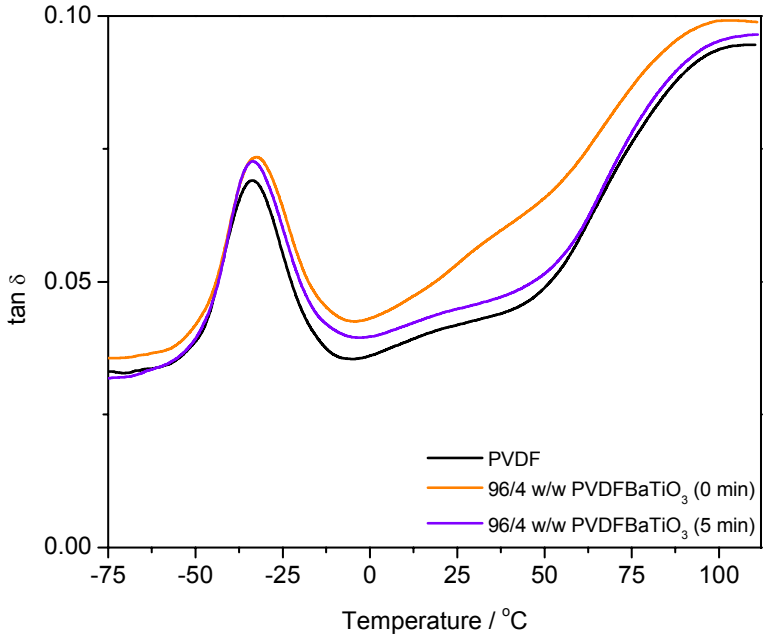

Figure 4.28 Damping factor as function of temperature of PVDF and the PVDF/$BaTiO_3$ nanocomposites

There was also an observable increase in the E' values of PVDF/PMMA when $BaTiO_3$ nanoparticles were present (Figures 4.29 to 4.31), but the increase was more when the 10 min. activated fillers were present. This is also the result of the larger specific surfaces, and stronger interactions with the polymer matrix, which enabled restricted movement of the polymer chains and an increase in the storage modulus.

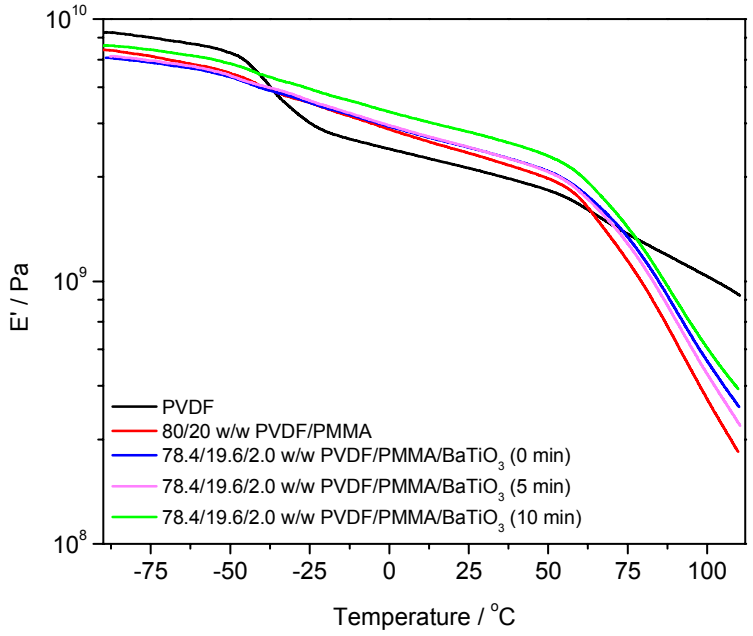

Figure 4.29 Storage modulus as function of temperature of PVDF, PVDF/PMMA and the PVDF/PMMA/$BaTiO_3$ nanocomposites

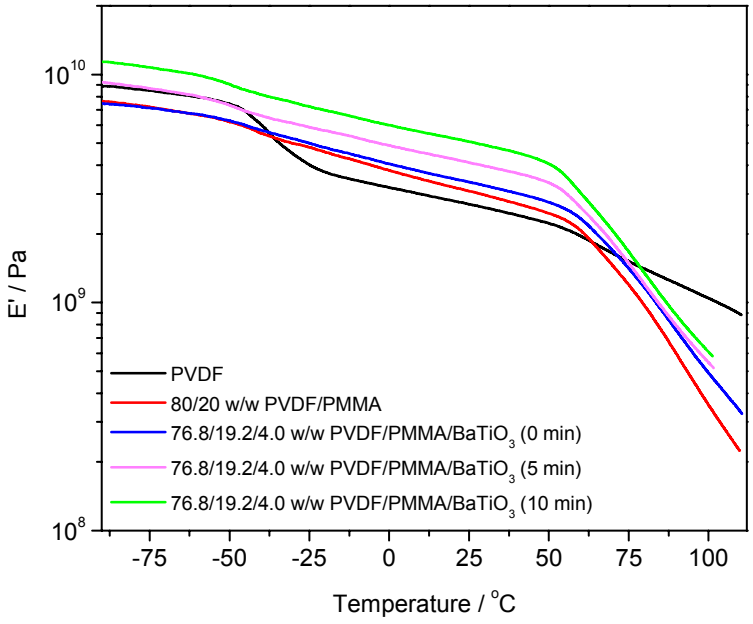

Figure 4.30 Storage modulus as function of temperature of PVDF, PVDF/PMMA and the PVDF/PMMA/$BaTiO_3$ nanocomposites

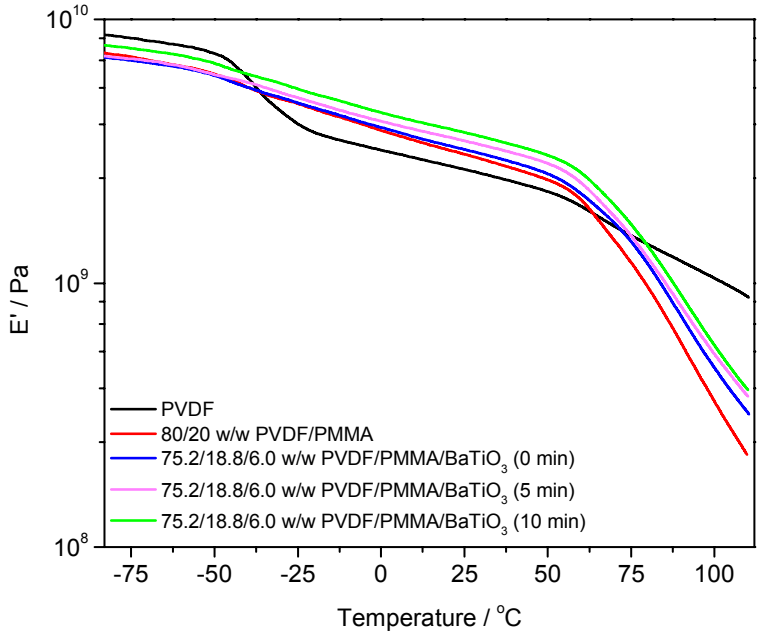

Figure 4.31 Storage modulus as function of temperature of PVDF, PVDF/PMMA and the PVDF/PMMA/$BaTiO_3$ nanocomposites

The tan δ curve of the blend (Figures 4.32 to 4.34) shows that the addition of PMMA to PVDF significantly decreased the intensity of α_a-relaxation peak and new peaks emerged at 15 and 95 °C. Motaung *et al.* [27] showed that the same PMMA used in this study has a T_g at 120 °C. The peak at 95 °C is at a lower temperature and should therefore be attributed to the segmental motions of a PVDF/PMMA amorphous phase rich in PMMA, and this peak overlaps with the α_c-relaxation peak of PVDF. The significantly reduced peak at -34 °C indicates that most of the amorphous PVDF formed partially miscible blends with PMMA. The partial miscibility in is the result of dipole/dipole interactions between the $>CF_2$ groups of PVDF and the >C=O groups of PMMA. This is confirmed by the appearance of the peak at 15 °C, which indicates the segmental motions of a PVDF/PMMA amorphous phase rich in PVDF. It does not seem as if the presence of the nanoparticles had much influence on the peak intensities of the peaks at -34 and 15 °C, but the intensity of the peak at 95 °C decreased for the samples containing the nanoparticles. This observation implies that the nanoparticles were either located on the PVDF/PMMA interphase or in the PMMA rich phase.

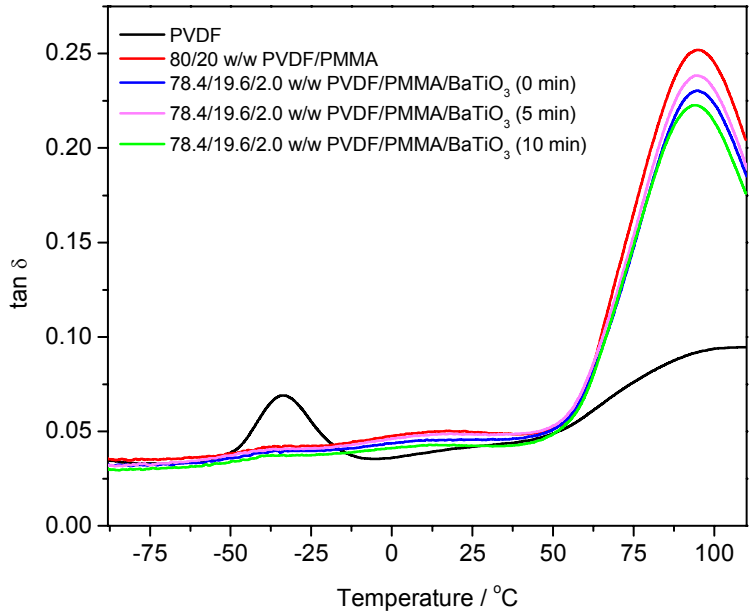

Figure 4.32 Damping factor as function of temperature of PVDF, PVDF/PMMA and the PVDF/PMMA/$BaTiO_3$ nanocomposites

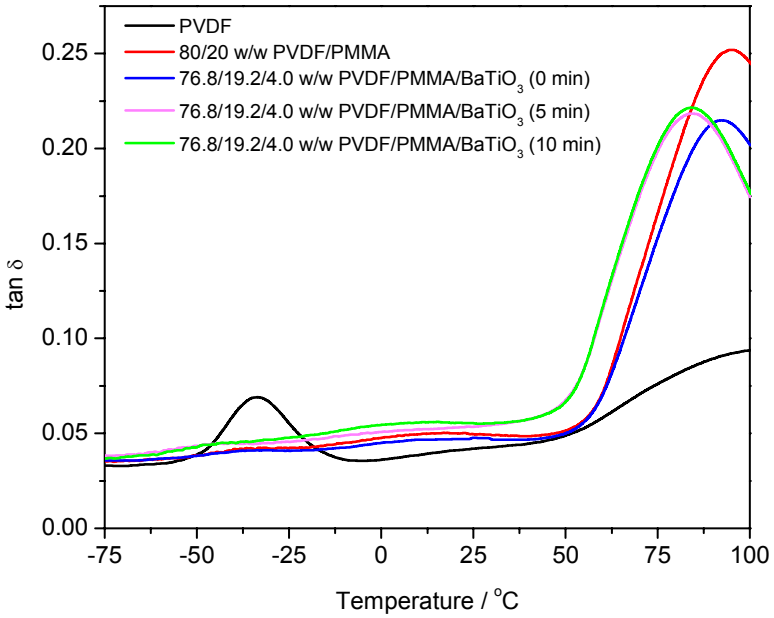

Figure 4.33 Damping factor as function of temperature of PVDF, PVDF/PMMA and the PVDF/PMMA/$BaTiO_3$ nanocomposites

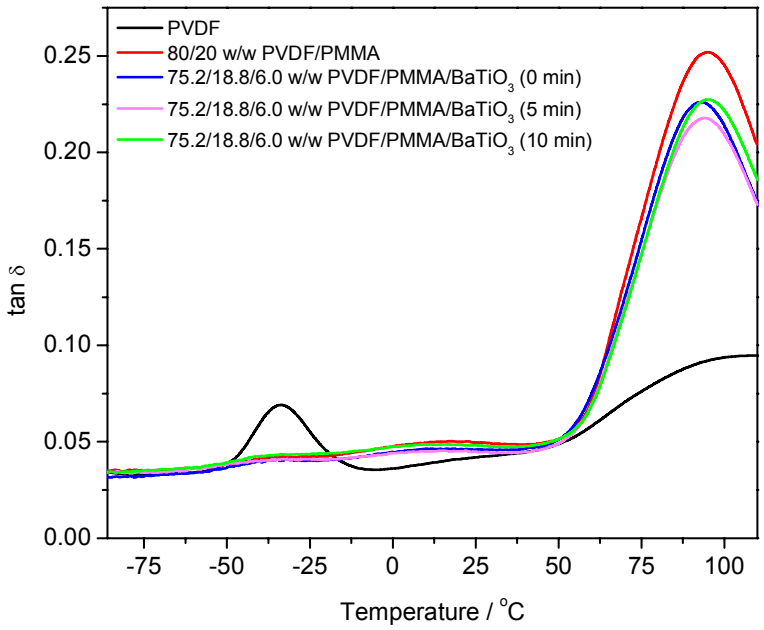

Figure 4.34 Damping factor as function of temperature of PVDF, PVDF/PMMA and the PVDF/PMMA/$BaTiO_3$ nanocomposites

4.8 Dielectric spectroscopy

The dielectric constants of PVDF, 80/20 w/w PVDF/PMMA and 78.4/19.6/2.0 w/w PVDF/PMMA/$BaTiO_3$ as function of temperature are shown in Figures 4.35 to 4.39. The effects of non-activated and mechanically activated $BaTiO_3$ nanoparticles on the dielectric constants (ε) of polymer matrices obtained at different frequencies are depicted in Figures 4.35 and 4.36. The dielectric permittivity and dielectric loss are denoted by ε' and ε" respectively. Generally, it is observable that the addition of PMMA to PVDF lowers the ε' and ε" values of PVDF. Meng *et al.* [28] investigated the effect of PMMA addition on the dielectric properties of PVDF and obtained similar results. They attributed this to the dilution effect of PMMA, which has a lower dielectric constant than PVDF.

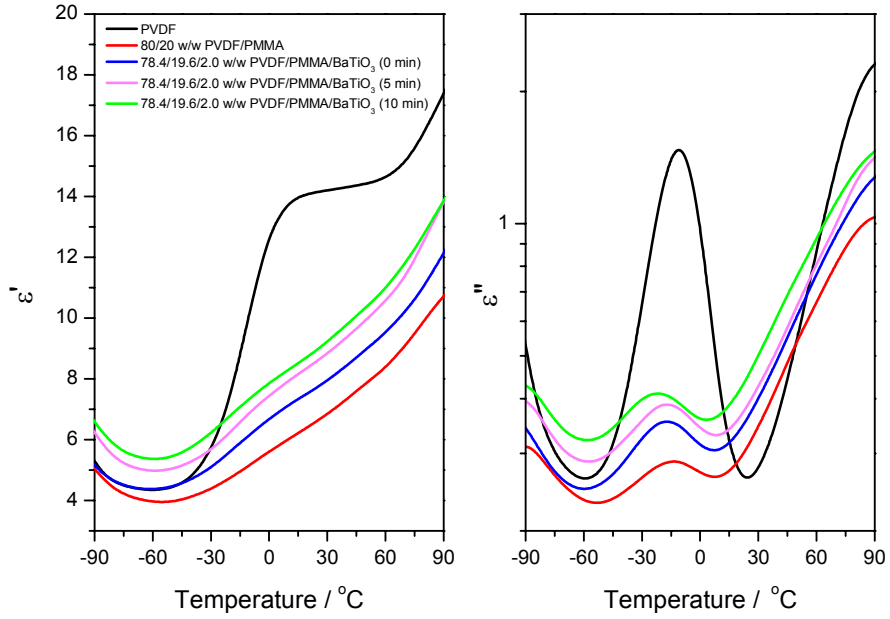

Figure 4.35 Dielectric spectra of PVDF, PVDF/PMMA and the PVDF/PMMA/$BaTiO_3$ nanocomposites obtained at a frequency of 180 Hz

There was an observable increase in the ε' and ε" values associated with PVDF/PMMA when $BaTiO_3$ nanoparticles were added, but the increase was more observable when the highly activated fillers were added. The higher ε' and ε" values of the 78.4/19.6/2.0 w/w PVDF/PMMA/$BaTiO_3$ (0 min) composite are attributed to the presence of the $BaTiO_3$ filler which has a higher dielectric constant than the 80/20 w/w PVDF/PMMA matrix. The higher ε' and ε" values of the 78.4/19.6/2.0 w/w PVDF/PMMA/$BaTiO_3$ (10 min) are attributed to the presence of a larger amount of β-phase crystals, as observed from the Raman results. The β-phase of PVDF is more important because of its high dielectric constant and piezoelectric properties [29]. Compared to the non-activated $BaTiO_3$ particles, the 10 minutes mechanically activated $BaTiO_3$ particles possess larger specific surfaces and defects, which facilitate the β-phase crystallization of PVDF. It is clear that the increase in the ε' and ε" values is either caused by an increase in $BaTiO_3$ content or an increase in the β-phase, or a combination of the two.

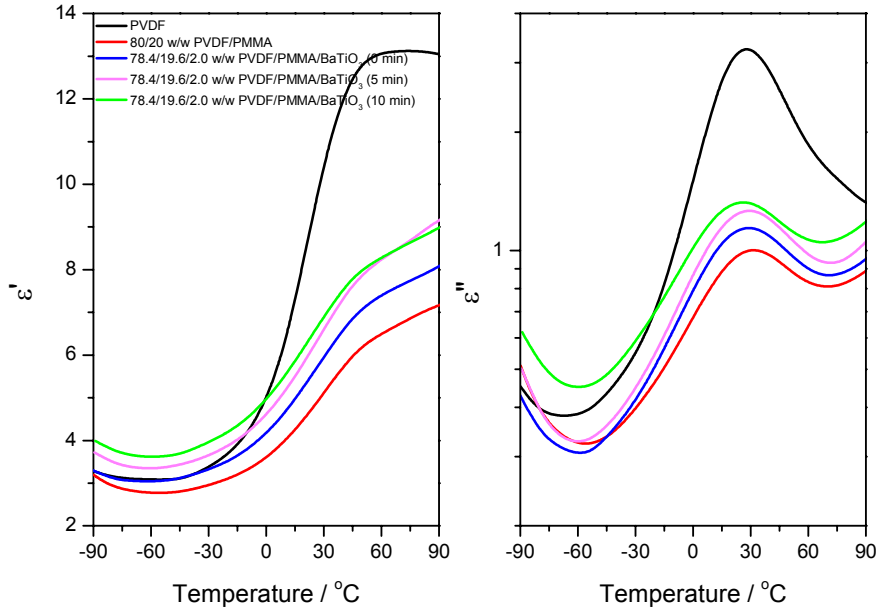

Figure 4.36 Dielectric spectra of PVDF, PVDF/PMMA and the PVDF/PMMA/$BaTiO_3$ nanocomposites obtained at a frequency of 180 kHz

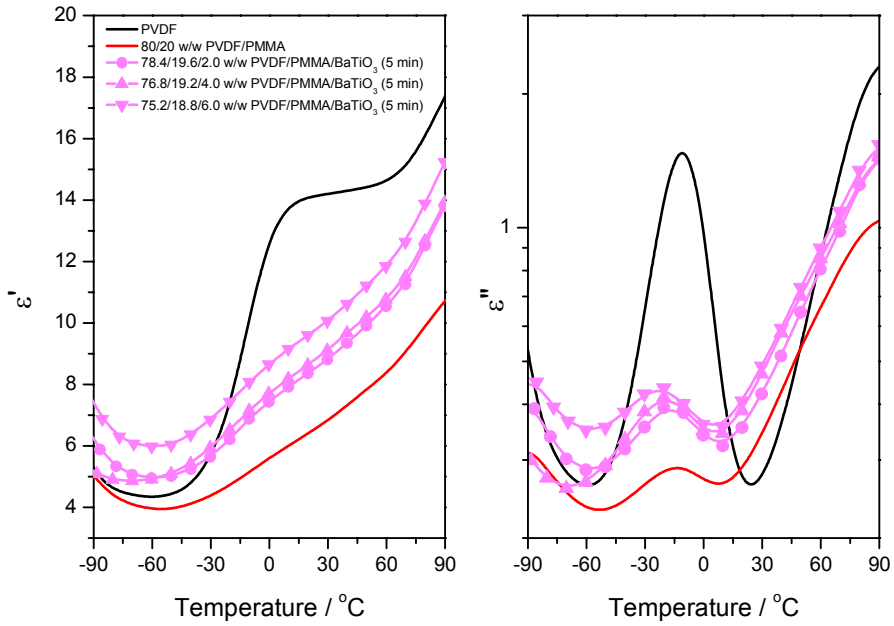

Figure 4.37 Dielectric spectra of PVDF, PVDF/PMMA and the PVDF/PMMA/$BaTiO_3$ nanocomposites obtained at a frequency of 180 Hz

The dielectric spectrum of PVDF has a relaxation between -30 and 30 °C, called the α_a-relaxation [30]. Mijovic *et al.* [31] associated the α_a-relaxation of pure PVDF with segmental motions in the amorphous phase, and the α_a-relaxation of PVDF/PMMA with local segmental motions in the crystal-amorphous interphase. The intensity of the α_a-relaxation peak of PVDF is decreased when PMMA is added, and this peak shifts to higher temperatures at very high frequencies. Ando *et al.* [32] suggested that the α_a-relaxation may also be related to the PVDF crystallites, as its intensity decreases with the addition of PMMA which lowers its crystallinity. The presence of $BaTiO_3$ in PVDF/PMMA slightly shifts the α_a-relaxation peak to lower temperatures, and this effect is more visible in the blend nanocomposites containing 10 min. activated $BaTiO_3$ nanoparticles. We have already shown that the presence of $BaTiO_3$ nanoparticles increases the β-crystal content of PVDF in PVDF/PMMA, and this will naturally influence the crystal-amorphous interphase, which is in this case seen as a shift in the α_a-relaxation peak. It is also observed that the ε' and ε'' values increase with an increase in mechanically activated $BaTiO_3$ content. Although we did not investigate the influence of the content of mechanically activated $BaTiO_3$ on the amount of β-phase crystals, we believe that larger amounts of mechanically activated $BaTiO_3$ nanoparticles induce more of the β-phase, hence the higher ε' and ε'' values.

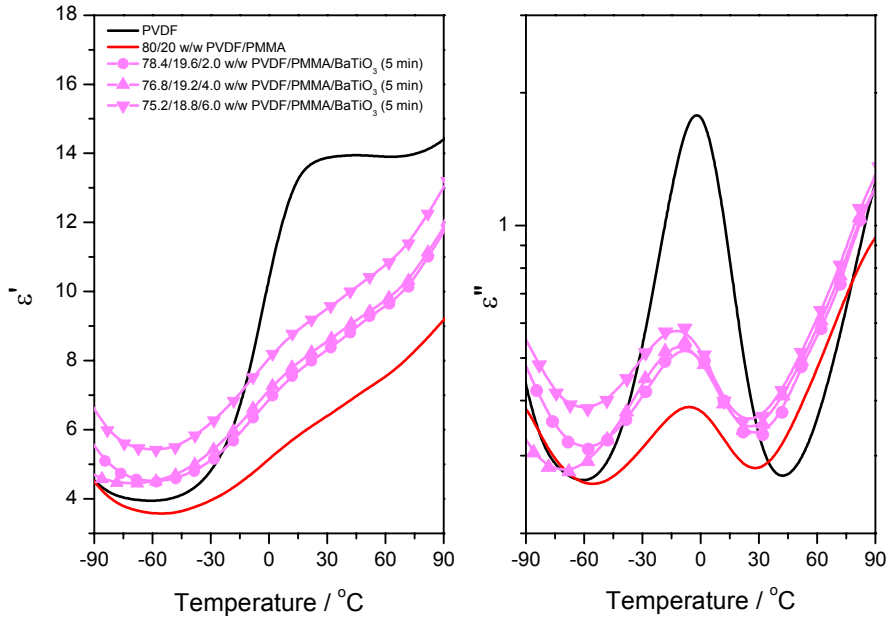

Figure 4.38 Dielectric spectra of PVDF, PVDF/PMMA and the PVDF/PMMA/$BaTiO_3$ nanocomposites obtained at a frequency of 1800 Hz

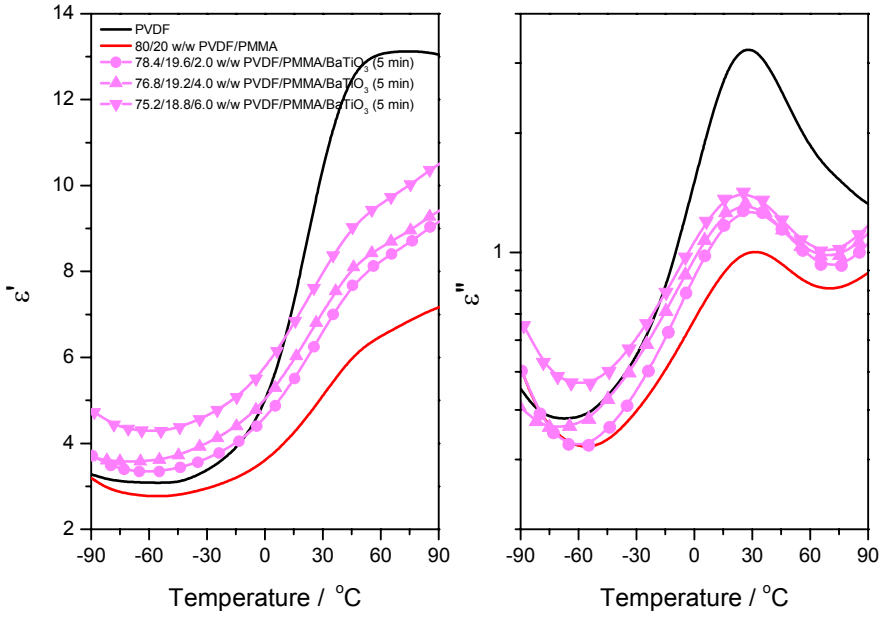

Figure 4.39 Dielectric spectra of PVDF, PVDF/PMMA and the PVDF/PMMA/$BaTiO_3$ nanocomposites obtained at a frequency of 180 kHz

4.9 References

[1] R. Gregorio Jr, N.C. Pereira de Souza Nociti. Effect of PMMA addition on the solution crystallization of the alpha and beta phases of poly(viny1idene fluoride) (PVDF). Journal of Physics D: Applied Physics 1995; 28:432-436.
DOI: 10.1088/0022-3727/28/2/028

[2] Y. Bormashenko, R. Pogreb, O. Stanevsky, E. Bormashenko. Vibrational spectrum of PVDF and its interpretation. Polymer Testing 2004; 23:791-796.
DOI: 10.1016/j.polymertesting.2004.04.001

[3] L. He, J. Sun, X. Wang, L. Yao, J. Li, R. Song, Y. Hao, Y. He, W. Huang. Enhancement of β-crystalline phase of poly(vinylidene fluoride) in the presence of hyperbranched copolymer wrapped multiwalled carbon nanotubes. Journal of Colloid and Interface Science 2011; 363:122-128.
DOI: 10.1016/j.jcis.2011.07.042

[4] B. Seyhan Ince-Gunduz, R. Alpern, D. Amare, J. Crawford, B. Dolan, S. Jones, R. Kobylarz, M. Reveley, P. Cebe. Impact of nanosilicates on poly(vinylidene fluoride) crystal polymorphism: Part 1. Melt-crystallization at high supercooling. Polymer 2010; 51:1485-1493.
DOI: 10.1016/j.polymer.2010.01.011

[5] J. Sun, L. Yao, Q.-L. Zhao, J. Huang, R. Song, Z. Ma, L.-H. He, W. Huang, Y.-M. Hao. Modification on crystallization of poly(vinylidene fluoride) (PVDF) by solvent extraction of poly(methyl methacrylate) (PMMA) in PVDF/PMMA blends. Frontiers of Materials Science 2011; 5:388-400.
DOI: 10.1007/s11706-011-0152-2

[6] R. Gregorio Jr. Determination of the α, β and γ crystalline phases of poly(vinylidene fluoride) films prepared at different conditions. Journal of Applied Polymer Science 2006; 100:3272-3279.
DOI: 10.1002/app.23137

[7] J.G. Lee, S.H. Kim, H.C. Kang, S.H. Park. Effect of TiO_2 on PVDF/PMMA composite films prepared by thermal casting. Macromolecular Research 2013; 21:349-355.
DOI: 10.1007/s13233-013-1017-6

[8] X. Zhao, J. Cheng, J. Zhang, S. Chen, X. Wang. Crystallization behavior of PVDF/PMMA blends prepared by in situ polymerization from DMF and ethanol. Journal of Materials Science 2012; 47:3720-3728.
DOI: 10.1007/s10853-011-6221-1

[9] M.Y.F. Elzayat, S. El-Sayed, H.M. Osman, M. Amin. X-ray diffraction and differential scanning calorimetry studies of a $BaTiO_3$/polyvinylidene fluoride composites. Polymer Engineering and Science 2012; 52:1945-1950.
DOI: 10.1002/pen.23132

[10] P. Durána, D. Gutierrez, J. Tartaj, M.A. Banãres, C. Moure. On the formation of an oxycarbonate intermediate phase in the synthesis of $BaTiO_3$ from (Ba,Ti)-polymeric organic precursors. Journal of the European Ceramic Society 2002; 22:797-807.
DOI: 10.1016/S0955-2219(01)00392-2

[11] V. Vinothini, P. Singh, M. Balasubramanian. Synthesis of barium titanate nanopowder using polymeric precursor method. Ceramics International 2006; 32:99-103.
DOI: 10.1016/j.ceramint.2004.12.012

[12] T.-C. Huang, M.-T. Wang, H.-S. Sheu, W.-F. Hsieh. Size-dependent lattice dynamics of barium titanate nanoparticles. Journal of Physics: Condensed Matter 2007; 19:1-12.
DOI: 10.1088/0953-8984/19/47/476212

[13] W.-S. Cho, E. Hamada. Synthesis of ultrafine $BaTiO_3$ particles from polymeric precursor: Their structure and surface property. Journal of Alloys and Compounds 1998; 266:118-122.
DOI: 10.1016/S0925-8388(97)00446-5

[14] J.Q. Qi, T. Peng, Y.M. Hu, L. Sun, Y. Wang, W.P. Chen, L.T. Li, C.W. Nan, H.L.W. Chan. Direct synthesis of ultrafine tetragonal $BaTiO_3$ nanoparticles at room temperature. Nanoscale Research Letters 2011; 6:1-4.
DOI: 10.1186/1556-276X-6-466

[15] A. Gajović, J.V. Pleština, K. Žagar, M. Plodinec, S. Šturm, M. Čeh. Temperature-dependent Raman spectroscopy of $BaTiO_3$ nanorods synthesized by using a template-assisted sol-gel procedure. Journal of Raman Spectroscopy 2013; 44:412-420.
DOI: 10.1002/jrs.4206

[16] S. Satapathy, S. Pawar, P.K. Gupta, K.B.R. Varma. Effect of annealing on phase transition in poly(vinylidene fluoride) films prepared using polar solvent. Bulletin of Materials Science 2011; 34:727-733.
DOI: 10.1007/s12034-011-0187-0

[17] P. Nallasamy, S. Mohan. Vibrational spectroscopic characterization of form II poly(vinylidene fluoride). Indian Journal of Pure and Applied Physics 2005; 43:821-827.

[18] M. Kobayashi, K. Tashiro, H. Tadokoro. Molecular vibrations of three crystal forms of poly(viny1idene fluoride). Macromolecules 1975; 8:158-171.
DOI: 10.1021/ma60044a013

[19] R.P. Vijayakumar, D.V. Khakhar, A. Misra. Phase transformation and enhancement of toughness in polyvinylidene fluoride by onium salts. Journal of Polymer Science Part B: Polymer Physics 2011; 49:1339-1344.
DOI: 10.1002/polb.22303

[20] I.-H. Kim, D.H. Baik, Y.G. Jeong. Structures, electrical, and dielectric properties of PVDF-based nanocomposite films reinforced with neat multi-walled carbon nanotube. Macromolecular Research 2012; 20:920-927.
DOI: 10.1007/s13233-012-0064-8

[21] R. Imamura, A.B. Silva, R. Gregorio Jr. γ to β phase transformation induced in poly(vinylidene fluoride) by stretching. Journal of Applied Polymer Science 2008; 110:3242-3246.
DOI: 10.1002/app.28851

[22] W. Li, H. Li, Y-M. Zhang. Preparation and investigation of PVDF/PMMA/TiO_2 composite film. Journal of Materials Science 2009; 44:2977-2984.
DOI: 10.1007/s10853-009-3395-x

[23] R.K. Layek, S. Samanta, D.P. Chatterjee, A.K. Nandi. Physical and mechanical properties of poly(methyl methacrylate)-functionalized graphene/poly(vinylidine fluoride) nanocomposites: Piezoelectric β polymorph formation. Polymer 2010; 51:5846-5856.
DOI: 10.1016/j.polymer.2010.09.067

[24] V. Sencadas, S. Lanceros-Méndez, J.F. Mano. Characterization of poled and non-poled β-PVDF films using thermal analysis techniques. Thermochimica Acta 2004; 424:201-207.
DOI: 10.1016/j.tca.2004.06.006

[25] L. Priya, J.P. Jog. Poly(vinylidene fluoride)/clay nanocomposites prepared by melt intercalation: Crystallization and dynamic mechanical behavior studies. Journal of Polymer Science: Part B: Polymer Physics 2002; 40:1682-1689.

[26] J.-W. Kim, W.-J. Cho, C.-S. Ha. Morphology, crystalline structure, and properties of poly(vinylidene fluoride)/silica hybrid composites. Journal of Polymer Science: Part B: Polymer Physics 2002; 40:19-30.
DOI: 10.1002/polb.10071

[27] T.E. Motaung, A.S. Luyt, F. Bondioli, M. Messori, M.L. Saladino, A. Spinella, G. Nasillo, E. Caponetti. PMMA-titania nanocomposites: Properties and thermal degradation behaviour. Polymer Degradation and Stability 2012; 97:1325-1333.
DOI: 10.1016/j.polymdegradstab.2012.05.022

[28] Q. Meng, W. Li, Y. Zheng, Z. Zhang. Effect of poly(methyl methacrylate) addition on the dielectric and energy storage properties of poly(vinylidene fluoride). Journal of Applied Polymer Science 2010; 116:2674-2684.
DOI: 10.1002/app.31777

[29] Y. Zhang, S. Jiang, M. Fan, Y. Zeng, Y. Yu, J. He. Piezoelectric formation mechanisms and phase transformation of poly(vinylidene fluoride)/graphite nanosheets

nanocomposites. Journal of Materials Science: Materials in Electronics 2013; 24:927-932.
DOI: 10.1007/s10854-012-0851-1

[30] L. Yu, P. Cebe. Effect of nanoclay on relaxation of poly(vinylidene fluoride) nanocomposites. Journal of Polymer Science: Part B: Polymer Physics 2009; 47:2520-2532.
DOI: 10.1002/polb.21864

[31] J. Mijovic, J.-W. Sy, T.K. Kwei. Reorientational dynamics of dipoles in poly(vinylidene fluoride)/poly(methyl methacrylate) (PVDF/PMMA) blends by dielectric spectroscopy. Macromolecules 1997; 30:3042-3050.
DOI: 10.1021/ma961774w

[32] Y. Ando, D.Y. Yoon. Phase separation in quenched noncrystalline poly(vinylidene fluoride)/poly(methyl methacrylate) blends. Polymer Journal 1992; 24:1329-1336.
DOI: 10.1295/polymj.24.1329

CHAPTER 5

CONCLUSIONS

PVDF/$BaTiO_3$ and PVDF/PMMA/$BaTiO_3$ samples were prepared by melt-mixing, quenching and annealing. In the PVDF nanocomposites, non-activated and mechanically activated $BaTiO_3$ nanoparticles had no significant influence on the formation of β-crystals. β-crystals formed when PVDF was blended with PMMA. The non-activated and mechanically activated $BaTiO_3$ nanoparticles influenced the formation of PVDF β-crystals in PVDF/PMMA in different ways. The non-activated $BaTiO_3$ nanoparticles reduced the formation of β-crystals, and this effect was more observable at higher loadings of non-activated $BaTiO_3$. The mechanically activated $BaTiO_3$ nanoparticles, however, improved the formation of β-crystals. This improvement was more prevalent at higher loadings of the 10 minutes mechanically activated $BaTiO_3$ nanoparticles. The setup which was found to be most effective in the formation of β-crystals is 75.2/18.8/6.0 w/w PVDF/PMMA/$BaTiO_3$ (10 min).

Both PVDF/PMMA and the PVDF/PMMA/$BaTiO_3$ (10 min) nanocomposites displayed a two-step degradation process, but the degradation of PVDF in the nanocomposites was more rapid due to the catalyzing effect of the filler. The melting temperatures of PVDF/PMMA and the PVDF/PMMA/$BaTiO_3$ (10 min) nanocomposites were very similar, despite different amounts of β-crystals in these samples. The PVDF/PMMA/$BaTiO_3$ (10 min) nanocomposites showed much higher storage modulus values than PVDF/PMMA because of the reinforcement of the blend by the nanosized $BaTiO_3$ filler. The PVDF/PMMA/$BaTiO_3$ (10 min) nanocomposites showed higher dielectric constants than PVDF/PMMA because of the higher β-crystal contents.

Although the main goal of this research was to improve piezoelectricity through increased β-crystal formation, it was not possible to measure the level of piezoelectricity in our samples because of logistical constraints. The piezoelectricity can be investigated by first poling the samples in silicon oil, followed by applying the desired electric field for 30 min at 110 °C and then for a further 30 min while cooling to 35 °C. The piezoelectric coefficient (d_{33}) can then be measured with a Berlincourt-type d_{33}-meter, which will be done during follow-up research.

ACKNOWLEDGEMENTS

I would like to thank God for giving me strength and courage for writing this thesis. Everything good that is happening in my life is the will of the Almighty God, and every path I take is His direction.

I am very grateful to my supervisors, **Prof. Adriaan Stephanus Luyt** and **Dr. Vladimir Djoković**, for their supervision, guidance, encouragement, criticism and patience especially during the hard times in this project. They have given me the best years as a student during the duration of this project.

I am very grateful to my friends and colleagues in the Polymer Research Group of UFS (Qwaqwa Campus) for the fruitful discussions on my project. Special thanks to Mr. Teboho Mokhena, Mr. Teboho Motsoeneng, Mr. Jonas Mochane, Dr. Duško Dudić, Dr. Essa Ahmad, Dr. Thabang Mokhothu, Ms. Puseletso Mofokeng, Ms. Motshabi Sibeko, Mr.Shale Sefadi, Mr. Mfiso Mngomezulu, Dr. Tshwafo Motaung, Dr. Nomampondomise Molefe, Mrs. Moipone Malimabe, Mr. Tsietsi Tsotetsi, Ms. Cheryll-Ann Clarke, Mr. Senzo Mdletse, Ms. Lerato Mollo, Ms. Thandi Gumede, Ms. Mamohanoe Molaba, Ms. Tshepiso Molaba. Mr. Bongani Msibi, Mr. Lucky Dlamini, Mr. Moeketsi Mangwaela, Ms. Nomadlozi Nhlapo.

Special thanks to the Mosia and Mojaki families for the constant love and support.

I would also like to thank the University of the Free State (UFS) and the National Research Foundation (NRF) for financial support.

Appendix A

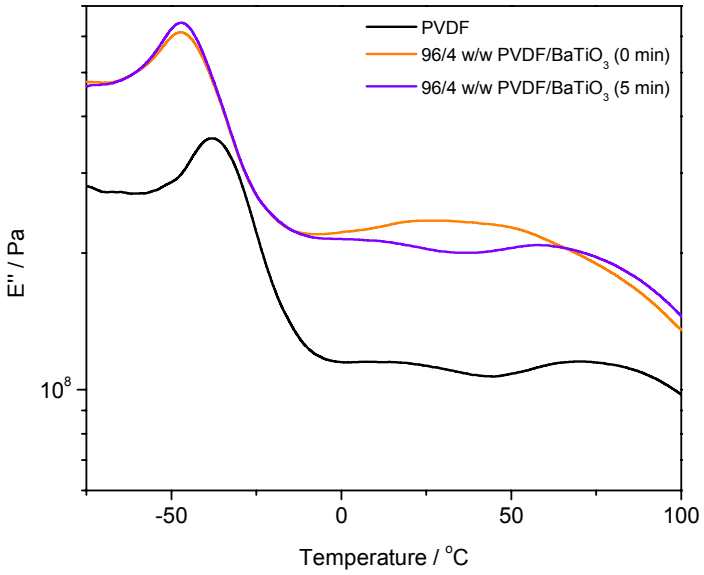

Figure A.1 Loss modulus as function of temperature of PVDF and the PVDF/$BaTiO_3$ nanocomposites

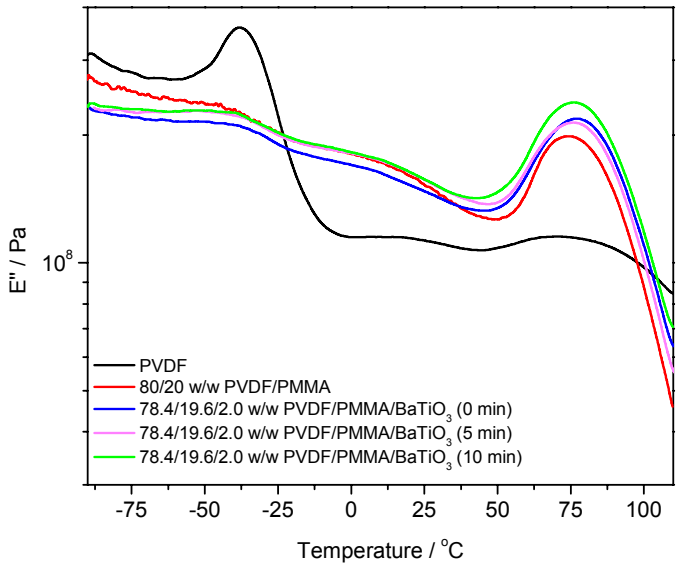

Figure A.2 Loss modulus as function of temperature of PVDF, PVDF/PMMA and the PVDF/PMMA/$BaTiO_3$ nanocomposites

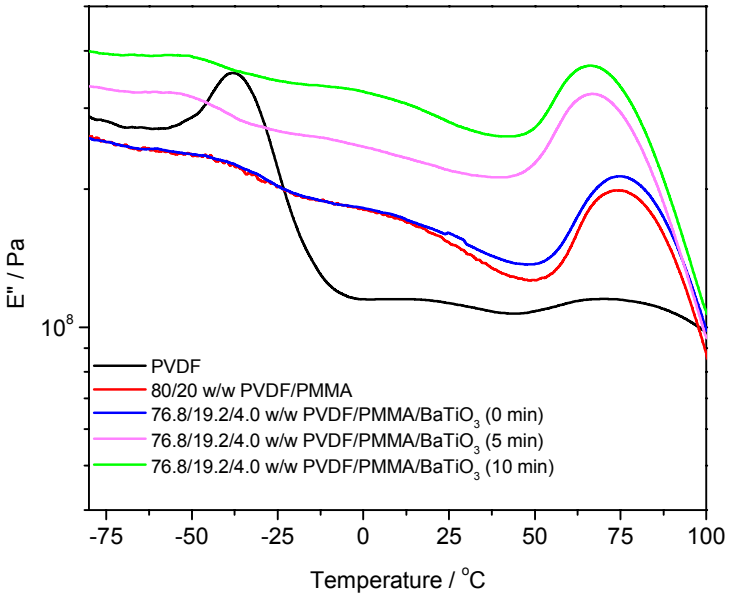

Figure A.3 Loss modulus as function of temperature of PVDF, PVDF/PMMA and the PVDF/PMMA/$BaTiO_3$ nanocomposites

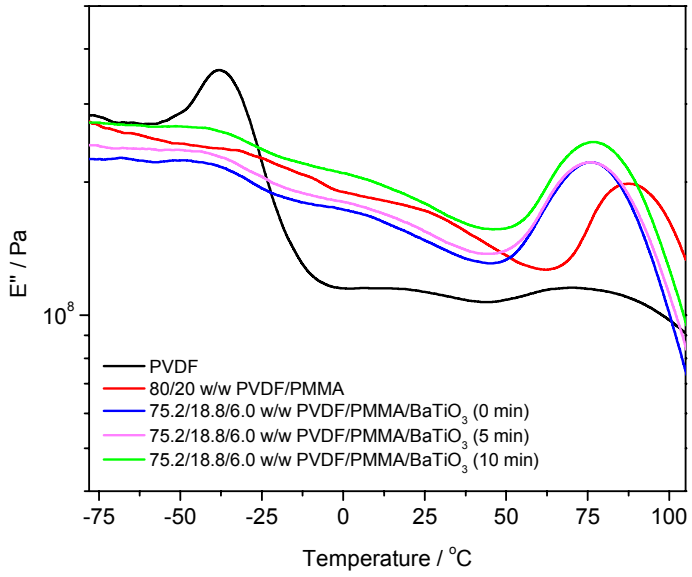

Figure A.4 Loss modulus as function of temperature of PVDF, PVDF/PMMA and the PVDF/PMMA/$BaTiO_3$ nanocomposites